The cation channel mechanisms of subthreshold inward depolarizing currents in the VTA dopaminergic neurons and their roles in the chronic-stress-induced depression-like behavior

Jing Wang[1,3], Min Su[1,4], Dongmei Zhang[1,5], Ludi Zhang[1], Chenxu Niu[1], Chaoyi Li[1], Shuangzhu You[1], Yuqi Sang[1], Yongxue Zhang[1,6], Xiaona Du[1], Hailin Zhang[1,2*]

[1]Department of Pharmacology; The Key Laboratory of Neural and Vascular Biology, Ministry of Education; The Key Laboratory of New Drug Pharmacology and Toxicology, Hebei Medical University, Shijiazhuang, Hebei, China
[2]Department of Psychiatry, The First Hospital of Hebei Medical University, Mental Health Institute of Hebei Medical University, China
[3]Department of Pharmacochemistry, Hebei University of Chinese Medicine, Shijiazhuang, Hebei, China
[4]Yiling Pharmaceutical Company, Shijiazhuang, Hebei, China
[5]Department of Clinical Pharmacy, Xintai Ninth Hoapital, Xintai, Hebei, China
[6]Department of Pharmacy, Handan First Hospital, Handan, Hebei, China

*** Correspondence:**
Hailin Zhang
zhanghl@hebmu.edu.cn

Abstract:

The slow-intrinsic-pacemaker dopaminergic (DA) neurons originating in the ventral tegmental area (VTA) is implicated in various mood- and emotion-related disorders, such as anxiety, fear, stress and depression. Abnormal activity of projection-specific VTA DA neurons is the key factor in the development of these disorders. Here, we describe the crucial role for the NALCN and TRPC6, non-selective cation channels in mediating the subthreshold inward depolarizing current and driving the firing of action potentials of VTA DA neurons in physiological condition. Furthermore, we demonstrate that down-regulation of TRPC6 protein expression in the VTA DA neurons likely contributes to the reduced activity of projection-specific VTA DA neuron in chronic mild unpredictable stress (CMUS) depressive mice. In consistent with this, selective knockdown of TRPC6 channels in the VTA DA neurons conferred mice with depression-like behavior. This current study suggests down-regulation of

TRPC6 expression/function is involved in reduced VTA DA neuron firing and chronic stress-induced depression-like behavior in the mouse models of chronic stress-induced depression.

Keywords: Ventral tegmental area, Dopaminergic neurons, Cation channels, NALCN, TRPC6 channel

Introduction

Dopaminergic (DA) neurons in the ventral tegmental area (VTA) play a key role in mood, reward and emotion-related behaviors[1]. These DA neurons project, through mesocorticolimbic dopaminergic system, to brain regions including the nucleus accumbens (NAc), medial prefrontal cortex (mPFC) and basolateral amygdala (BLA), and modulate these target neuronal circuits through their regulated activity (firing of action potentials)[2, 3]. As such, understandably, the altered functional activity of the VTA DA neurons is found to be the key determinants in abnormal behaviors related to the diseased conditions such as depression- or anxiety-related states[4]. Thus, the study on the mechanism underlying the firing activity of the VTA DA neurons is crucial for understanding the function of the DA circuitry and the pathogenesis of related mental diseases[4-8].

The VTA DA neurons are slow intrinsic pacemakers, which are further modulated by synaptic inputs from multiple excitatory and inhibitory projections [9, 10]. Firing activity controls the release of DA, thus function of the VTA DA neurons. The altered activity of the VTA DA neurons in a pathological state includes altered firing frequency and switch of the firing patterns[7, 11].

The research on the mechanism for spontaneous firing of action potential (AP) is the key to understand functional regulation of the VTA DA neurons. A variety of ion channels (e.g. voltage-gated Na^+ channels, high-threshold-activated Ca^{2+} channels, Kv2, large conductance calcium-activated potassium channels, A- and M-type potassium channels) are reported to be involved in regulation of the spontaneous firing activity of midbrain DA neurons (including the substantial nigra pars compacta, SNc and VTA)[12-22]. However, it is not completely clear how this spontaneous firing is initiated. AP fires when the resting membrane potential (RMP) is depolarized

to the activation threshold for the voltage-dependent Na^+ channels, which results in opening of Na^+ channels and the upstroke of AP[12]. Therefore, a controlled depolarization of the RMP to the activation threshold of AP is the first key step in a cascade leading to firing of AP. In the VTA DA neurons, the identity of ion channels contributing to this subthreshold depolarization has not been unambiguously established.

In some cells with spontaneous firing of AP, such as cardiomyocytes and certain neurons (including a subset of midbrain SNc DA neurons[23]), the ionic mechanism for the auto-rhythmicity is the HCN, a non-selective cation channel that would depolarize the membrane potential after being activated at a hyperpolarized membrane potential[23]. However, in the VTA DA neurons, results concerning the HCN channels to the spontaneous firing are controversial[15, 23-25].

Another non-selective cation channel, NALCN, unlike HCN, is a non-voltage dependent channel[26], and is reported to be among the candidates for molecular correlates of the persistent background Na^+ leak currents in the VTA DA neurons [27, 28]. The NALCN-mediated background Na^+ leak currents are found to be involved in modulation of firing activity in a variety of neurons including DA neurons in the SNc[26, 28-31]. However, it has not been reported if NALCN plays a role in spontaneous firing of the VTA DA neurons, although the VTA DA neurons have larger Na^+ leak currents than SNc DA neurons do[15].

TRP channels are a large class of non-selective cation channels, and are widely distributed in the peripheral and central nervous system. TRPC3, which has a high homology with TRPC6[32], is found to be involved in the regulation of cardiac and SNc DA neuronal excitability, generating depolarizing currents, triggering action potentials and participating in cellular rhythmic firing[31, 33, 34].The role of TRP channels, except TRPC4[35], in the regulation of VTA DA neuronal excitability has not been described.

In this study, we drove to find channel conductance which contribute to the subthreshold depolarization and thus the spontaneous firing of the VTA DA neurons. And furthermore, we investigated if these channels are the molecular mechanism for the altered function activity of the VTA DA neurons related to depression-like

behaviors in mouse model of depression. We started by profiling the expression of non-selective cation channels (NSCCs) of the VTA DA neurons using method of Patch-Seq from midbrain DA neurons projecting to different brain regions, and then focused on HCN, NALCN, TRPC6 and TRPV2 channels which are dominantly expressed in these DA neurons.

Results

Inflow of extracellular Na^+ contribute to the subthreshold depolarization of the VTA DA neurons

One key feature of the midbrain DA neurons is that these neurons are relatively depolarized in the resting condition; the resting membrane potential (RMP) is far from the K^+ equilibrium potential (~-55 mV *vs* ~-90 mV)[15], which enable the spontaneous firing. Thus, there must be persistent inward depolarizing conductance counterbalancing the hyperpolarizing K^+ conductance which otherwise would maintain the RMP at a hyperpolarized level. The main aim of this study is to identify the subthreshold depolarizing conductances which contribute to the spontaneous firing of the VTA DA neurons. While we initially performed our experiments using male mice, most of the experiments were also repeated using female mice, results of which were reported separately in the following results. We first observed firing frequency and the RMP of the VTA DA neurons using patch clamp recordings. The midbrain DA neurons, marked by dopamine transporter (DAT), mainly located in the VTA and SNc (**Fig. 1Ai**). We recorded neurons from the VTA brain slices of mice, and performed single-cell PCR post electrophysiologic recordings to identify the DA neurons with established markers for DA neurons (TH, DAT, D_2R (type2 dopamine receptor), and GIRK2 (G protein-gated inward rectifier K inwardly rectifying K^+ channels)). Although the majority of cells in the VTA area are DA neurons (~60%), there are still about 30% GABA neurons and a small number of glutamatergic neurons [36, 37]. Glutamatergic- and GABAergic neurons were also single-cell PCR typed by using markers of vGluT2 (vesicular glutamate transporter 2) and GAD1 (glutamic acid decarboxylase 1), respectively (**Fig. 1Aii**).

To focus on the intrinsic channel conductance for spontaneous firing, potential input modulation from fast-type transmitter transmission to the VTA DA neurons, namely

activation of AMPA/kainite/NMDA receptor and $GABA_A$ receptor were blocked by receptor antagonists CNQX, DL-AP5 and picrotoxin [15], respectively, in the following experiments.

We first studied whether inflow of extracellular Ca^{2+} contributed to initiation of spontaneous firing in the VTA DA neurons. It has been shown that, unlike the SNc DA neurons, the VTA DA neurons do not have subthreshold Ca^{2+} oscillatory waves[15], suggesting that subthreshold Ca^{2+} should not be an important component of subthreshold depolarizing conductance in the VTA DA neurons. In line with this finding, we found in our study, replacing Ca^{2+} with Mg^{2+} from the extracellular recording solution (ACSF, artificial cerebral spinal solution) did not reduce, but rather instead, increased the firing frequency of the VTA DA neurons in male mice (**Fig. 1B**, from 1.71 ± 0.19 Hz to 2.36 ± 0.28 Hz, n = 16, N = 8, $P < 0.001$). Consistent with this, the RMP of the VTA DA neurons was not hyperpolarized by replacing Ca^{2+} with Mg^{2+} from ACSF (**Fig. 1C**, from -50.77 ± 0.85 mV to -49.47 ± 1.09 mV, n = 14, N = 8, $P < 0.05$).

We then, in comparison with Ca^{2+}, observed the role of extracellular Na^+ in the RMP of the VTA DA neurons. For this, we followed the method of a previous study[15], by replacing Na^+ in ACSF with NMDG (N-methyl-d-glucamine); TTX (Tetrodotoxin) was also added to block the TTX-sensitive Na^+ currents, which is known to be the main contributor to the suprathreshold depolarization component of the action potential. Replacement of the extracellular Na^+ with NMDG resulted in a hyperpolarization of the RMP in mice (from -46.32 ± 1.97 mV to -64.53 ± 1.74 mV, n = 8, N = 5, $P < 0.001$, **Fig. 1D**), indicating a persistent inflow of Na^+ through a TTX-insensitive conductance which caused significant depolarization of the neurons, contributing significantly to the subthreshold depolarization of the VTA DA neurons. Similar results were obtained in the VTA DA neurons of female mice, with increased firing frequency and hyperpolarized RMP when the extracellular $Ca^{2+}$and Na^+ were replaced, respectively (**sFig. 1A** and **B**).

Taken together, above results indicate persistent Na^+ influx contribute to the subthreshold depolarization of the VTA DA neurons.

158 **Potential candidates of channel conductance contributing to subthreshold**
159 **depolarization of the VTA DA neurons**
160 The channel conductance mediating the above-described persistent Na^+ influx should
161 come from a cation channel(s) permeating to Na^+. We thus investigated the presence
162 and expression level of non-selective cation channels (NSCCs) in the VTA DA
163 neurons using a combination of patch clamp and single-cell RNA-Seq (Patch-seq)
164 technology[38]. In this part of the study, we considered the heterogeneity and
165 projection-specificity of the VTA DA neurons, i.e. VTA DA neurons projecting to
166 different brain regions have different electrophysiological characteristics[39]. Using
167 retrograde labelling techniques using retrobeads, sixty male VTA neurons projecting
168 to five different brain regions (medial prefrontal cortex, mPFC; basal lateral amygdala,
169 BLA; nucleus accumbens core, NAc c; nucleus accumbens lateral shell, NAc ls;
170 nucleus accumbens medial shell, NAc ms) (**sFig. 2**) were collected for RNA-Seq,
171 using patch-clamp electrodes. Consistent with previous study[39], the VTA DA
172 neurons projecting to above different brain regions were anatomically congregated
173 into subregions of the VTA (**sFig. 3)**. The high expression of biomarkers (Tyrosine
174 hydroxylase, TH; Dopamine decarboxylase, Ddc and Dopamine transporter, DAT) in
175 the 45 cells of 60 cells (**Fig. 2A**) indicates that these are DA neurons. In addition, less
176 than half of sequenced DA neurons (predominantly those projecting to NAc ms, BLA,
177 and mPFC) have biomarkers (Vesicular glutamate transporter, VGluT1-3) of
178 glutamatergic neurons, predicting a possible coexistence of neurotransmitters (DA and
179 glutamate)[40]. In contrast, fewer GABAergic neuronal markers (Glutamic acid
180 decarboxylase, GAD1/2 and vesicular GABA transporter, VGAT) co-expressed with
181 the DA neurons, which is consistent with previous studies that VTA DA neurons
182 co-expressing GABAergic neuronal markers mainly project to the lateral
183 habenula[41]. It needs to be noted that some neurons in the VTA only expressed
184 markers for glutamatergic or GABAergic neurons, these neurons were excluded from
185 further analysis as we focused our study on the DA neurons.
186 Expression levels of NSCCs in the VTA DA neurons classified by projection
187 specificity were analyzed and shown in **Fig. 2B**. Different colored strips on the top of
188 the figure corresponded to the projection specificity coded by the same colors in **Fig.**

189 **2A**. Multiple transient receptor potential channels (TRP) were present in the VTA DA
190 neurons, with prominent expression level of TRPC6 and TRPV2 (**Fig. 2Bi**). Other
191 prominently expressed NSCCs included HCN2, HCN3, NALCN and pannexin 1
192 (Panx1) (**Fig. 2Bii**). Summarized averaged relative expression levels for eight most
193 richly expressed NSCCs were shown in **Fig. 2Biii**. Furthermore, projection-specific
194 expression of these dominantly expressed NSCCs were analyzed and shown in **Fig.**
195 **2C**; interestingly only TRPC6 seemed expressed in a projection-specific manner,
196 namely, the VTA DA neurons projecting to the NAc have higher TRPC6 expression
197 than the VTA DA neurons projecting to the BLA and the mPFC **(Fig. 2C**). In our
198 subsequent study, we focused our study on HCN, NALCN, TRPC6 and TRPV2, one
199 for they are the prominently expression channels, and two for some of these channels
200 have been indicated in modulation of excitability of different neuron types[23, 24, 26,
201 28-31, 42]. Panx1 was investigated in a separate study since it normally composes the
202 semi channels which are different from these more conventional ion channels.
203
204 **HCN does not contribute to the spontaneous firing of the VTA DA neurons**
205 We mainly used two pharmacological tools as HCN channel blockers, CsCl and
206 ZD7288[15, 24] to explore the role of HCN channels in the spontaneous firing of the
207 male VTA DA neurons. Efficient blocking effect of these blockers on HCN channel
208 was first verified. For this, the sag potential produced by a hyperpolarizing current
209 (-100 pA) injection was used to assess HCN activity[24]. Both CsCl (3 mM) and
210 ZD7288 (60 μM) effectively reduced the sag potential (from 16.43 ± 2.96 mV to 3.84
211 ± 1.92 mV, n = 4, N = 4, $P < 0.05$; from 19.38 ± 3.14 mV to 4.18 ± 2.60 mV, n = 4, N
212 = 4 respectively, $P < 0.05$) (**sFig. 4A and B**).
213 However, these same HCN blockers did not inhibit the spontaneous firing of the VTA
214 DA neurons; CsCl slightly increased (1.96 ± 0.19 Hz to 2.14 ± 0.34 Hz, n = 7, N = 4)
215 whereas ZD7288 slightly decreased the firing frequency (1.65 ± 0.25 Hz to 1.50 ±
216 0.24 Hz, n = 13, N = 5), but none of these effects were statistically significant ($P >$
217 0.05) (**sFig. 4C and D)**. It has been reported that VTA DA neurons projecting to the
218 NAc lateral shell have more pronounced HCN/Ih currents than other VTA DA
219 neurons[39]. However, even the VTA DA neurons projecting to the NAc lateral shell

(retrogradely labelled by retrobeads), no effect of CsCl or ZD7288 on the spontaneous firing of the male VTA DA neurons were observed (from 2.04 ± 0.24 Hz to 1.93 ± 0.22 Hz, n = 5, N = 4, by CsCl, and from 1.71 ± 0.29 Hz to 1.65 ± 0.33 Hz, n = 5, N = 5, by ZD7288, $P > 0.05$) (**sFig. 5A and B**).

HCN are activated by membrane hyperpolarization, with an activation threshold around -70 ~ -90 mV (HCN2, HCN3)[43, 44]. At a depolarized RMP like these in the VTA DA neurons (-51.28 ± 1.85 mV, n = 8, N = 8; e.g. -54.50 mV, **sFig. 4Ai**, and -53.50 mV, **sFig. 4Bi**), HCN are most likely not activated thus would not participate in generation of spontaneous firing. To further prove this, we tested if a more hyperpolarized RMP would involve HCN in the spontaneous firing of the VTA DA neurons. For this, we first lowered the K^+ concentration in the extracellular ACSF from 3 mM to 1.5 mM to increase the gradient between inside and outside cellular K^+; this maneuver indeed hyperpolarized the cell membrane from -53.33 ± 2.79 mV to -65.00 ± 3.02 mV (n = 6, N = 6, $P < 0.01$) (**sFig. 5C**). Interestingly, under 1.5 mM extracellular K^+, the spontaneous firing of the male VTA DA neurons was almost totally blocked by ZD7288 (**sFig. 5D**), although an initial enhancement was seen in some neurons (**sFig. 5Di**).

We tested another possible mechanism for HCN's failure to participate in generation of VTA DA firing. It has been reported that in the midbrain SNc DA neurons, HCN is involved in the spontaneous firing in young but not in adult mice, due to a more hyperpolarization-shifted activation threshold of HCN in SNc DA neurons in adult mice. We tested if this could also be the case in the VTA DA neurons. Indeed, as shown in **sFig. 5E**, in contrast to what we saw in adult male mice, the spontaneous firing frequency of the VTA DA neurons in young male mice (less than 15 days postnatal) was significantly reduced by ZD7288 (from 1.86 ± 0.29 Hz to 0.98 ± 0.24 Hz, n = 9, N = 5, $P < 0.05$).

Taken together, above results suggest HCN is not involved in the spontaneous firing of the VTA DA neurons in adult mice, due to a depolarized RMP and a hyperpolarization-shifted activation property.

NALCN contributes to subthreshold depolarization and spontaneous firing of the VTA DA neurons

The Na^+ currents produced by NALCN have been suggested to be an important component of background Na^+ currents in multiple central neurons including DA neurons in the substantia nigra[28].We next investigated if NALCN also play a role in setting the RMP and in the spontaneous firing of the VTA DA neurons. Consistent with above RNA-Seq results, both immunofluorescence (**Fig. 3A**) and single-cell PCR (**Fig. 3B)** results confirmed broad expression of NALCN in the VTA DA neurons.

$GdCl_3$ (100 μM), a nonspecific NALCN blocker [29, 30], hyperpolarized the RMP of the VTA DA neurons from -52.17 ± 4.15 mV to -67.33 ± 2.68 mV (n = 6, N = 6, $P < 0.05$) (**Fig. 3C**), reduced the spontaneous firing frequency of the VTA DA neurons from 1.89 ± 0.29 Hz to 1.32 ± 0.37 Hz (n = 7, N = 3, $P < 0.01$) (**Fig. 3D**). L703,606, a specific NALCN blocker[31], also hyperpolarized the RMP of the VTA DA neurons from -49.16 ± 1.48 mV to -54.30 ± 1.67 mV (n = 6, N = 4, $P < 0.001$) **(Fig. 3E)**, reduced the spontaneous firing frequency of the VTA DA neurons from 2.36 ± 0.38 Hz to 0.64 ± 0.32 Hz (n = 8, N = 4, $P < 0.001$) (**Fig. 3F**).

To observe a more specific effect on NALCN, a shRNA against NALCN was used to knockdown NALCN. For this, AAV9 viral construct (AAV9-U6-shRNA (NALCN)-CMV-GFP) was injected into the VTA of a mouse; similar AAV viral construct containing scramble-shRNA of nonsense sequences was utilized as controls. The qPCR results show sufficient knockdown of NALCN mRNA (NALCN-shRNA: 0.32 ± 0.07, N = 6; control scramble-shRNA: 1.07 ± 0.19, N = 6, $P < 0.01$, **Fig. 3G**) in the VTA tissue. Immunofluorescence results (**Fig. 3H**) show efficient infection of the VTA DA neurons (GFP expression in the DAT-positive neurons) by the virus. Knockdown of NALCN in the VTA DA neurons by shRNA almost completely silenced the firing of the male VTA DA neurons (0.07 ± 0.04 Hz *vs* 1.84 ± 0.25 Hz in shRNA (n = 12, N = 3) and scramble-shRNA (n = 10, N = 3) infected VTA DA neurons, respectively, $P < 0.001$, **Fig. 3I**). Furthermore, the RMP of the male VTA DA neurons was significantly hyperpolarized (-60.67 ± 2.33 mV *vs* -48.9 ± 1.45 mV in shRNA and scramble-shRNA infected VTA DA neurons, respectively, n = 18 and 15,

281 N = 5 and 5, $P < 0.001$, **Fig. 3J**). In female mice, L703,606 also reduced the
282 spontaneous firing frequency of the VTA DA neurons and knockdown of NALCN
283 also silenced the firing of the VTA DA neurons (**sFig. 6A** and **B**).
284 Taken together, above results suggest that NALCN is a major contributor to the
285 subthreshold depolarization and contribute significantly to the generation of
286 spontaneous firing in the VTA DA neurons.
287
288 **TRPC6 contributes to subthreshold depolarization and spontaneous firing of the**
289 **VTA DA neurons**
290 Above RNA-Seq results suggest a broad and strong expression of TRPC6 and TRPV2
291 channels in the VTA DA neurons. This part of the experiments was focused on the
292 role of these two TRP channels in subthreshold depolarization and spontaneous firing
293 of the VTA DA neurons.
294 Consistent with the RNA-Seq results, single-cell PCR experiments confirmed high
295 proportion expression of TRPC6 and TRPV2 in the VTA DA neurons (**Fig. 4A**);
296 among the 28 VTA DA neurons (DAT^+), 20 neurons expressed TRPV2 (71.4%), and
297 18 neurons (64.3%) expressed TRPC6. TRPC3, which is highly homologous with
298 TRPC6[45] and has been reported to be involved in the firing activity of the SNc DA
299 neurons[31], was not detected in RNA-Seq study (**Fig. 2B**), nor in the single-cell PCR
300 experiment (**Fig. 4A**). These results reciprocally confirmed the reliability of both
301 RNA-Seq and single cell PCR results.
302 General roles of TRP channels in subthreshold depolarization and spontaneous firing
303 of the VTA DA neurons were first assessed using a non-specific broad-spectrum TRP
304 channel blocker, 2-aminoethoxydiphenylborane (2-APB; 100 μM) and a specific
305 TRPC6 channel blocker, larixyl acetate[46] (LA; 10 μM). Both blockers significantly
306 reduced the firing frequency of the male VTA DA neurons (2-APB: from 1.32 ± 0.27
307 Hz to 0.06 ± 0.02 Hz, n = 12, N = 5, $P < 0.001$; LA: from 1.16 ± 0.21 Hz to 0.39 ±
308 0.09 Hz, n = 7, N = 5, $P < 0.01$; **Fig. 4B, 4C**). Accordingly, both blockers also
309 significantly hyperpolarized the RMP of the male VTA DA neurons (2-APB: from
310 -51.01 ± 2.20 mV to -61.64 ± 1.28 mV, n = 6, N = 6, $P < 0.001$; LA: from -53.93 ±
311 1.05 mV to -57.48 ± 1.09 mV, n = 5, N = 4, $P < 0.01$; **Fig. 4D, 4E**).

312 We then tested a more TRPV channel-selective blocker ruthenium red (RR), to study
313 possible role of TRPV2 (and other TRPV) in the spontaneous firing of the VTA DA
314 neurons. RR (60 μM), on average statistically, did not affect the spontaneous firing of
315 the male VTA DA neurons (from 2.30 ± 0.31 Hz to 2.18 ± 0.32 Hz, n = 9, N = 6, $P >$
316 0.05) (**sFig. 7**). However, it needs to be noted that among the nine VTA DA neurons
317 we tested, both increase (**sFig. 7B**) and decrease (**sFig. 7C**) of firing frequency by RR
318 were seen, thus with opposite changes of firing frequency in different populations of
319 neurons (**sFig. 7A**), no overall effect of RR was obtained from the current analysis.
320 We then focused our next study on TRPC6. Consistent with both RNA-Seq (**Fig. 2B**)
321 and single-cell PCR (**Fig. 4A**) results, the mRNA level of TRPC6 in mPFC-projecting
322 VTA single DA neuron is significantly lower than that in NAc c-projecting VTA
323 single DA neuron (0.56 ± 0.12, n = 25, N = 8 for mPFC-projecting TH-positive cells
324 *vs* 1.09 ± 0.10, n = 28, N = 7 for NAc c-projecting TH-positive cells,** $P < 0.01$, **Fig.**
325 **5A**) The immunofluorescence results also demonstrated strong expression of TRPC6
326 protein in the VTA DA neurons (**Fig. 5B**, TH-positive). A AAV viral construct with
327 shRNA against TRPC6 (AAV9-U6-shRNA (TRPC6)-CMV-GFP) was injected into
328 the VTA of mice, to knockdown TRPC6; efficiency of this knockdown was assessed
329 by using qPCR measuring the mRNA level of TRPC6 in the VTA tissue (**Fig. 5C**),
330 and efficiency of viral infection into the VTA DA neurons (marked by DAT) was
331 observed through visualization of GFP (**Fig. 5D**). Both qPCR (**Fig. 5C**) and
332 immunofluorescence (**Fig. 5D**) results indicated a sufficient repression of TRPC6 in
333 the VTA DA neurons. Indicative of a significant role in the spontaneous firing and
334 subthreshold depolarization, knockdown of TRPC6 (TRPC6-KD) resulted in a
335 substantial reduction in the spontaneous firing frequency (0.80 ± 0.25 Hz, n = 9, N=3
336 for TRPC6-KD *vs* 1.90 ± 0.27 Hz, n = 9, N = 3 for scramble-shRNA, $P < 0.01$, **Fig.**
337 **5E**), and hyperpolarization of the RMP (-58.21 ± 1.79 mV, n = 10, N = 6 for
338 TRPC6-KD *vs* -50.02± 0.67 mV, n = 10, N = 6 scramble-shRNA, $P < 0.001$, **Fig. 5G**)
339 of the male VTA DA neurons. In addition, the inhibitory effect of 2-APB and LA on
340 the firing of VTA DA neurons infected with TRPC6-shRNA largely diminished, with
341 no statistical difference in firing frequency before and after dosing (2-APB: from 0.58
342 ± 0.15 Hz to 0.40 ± 0.15 Hz, n = 7, N = 5, $P > 0.05$, **Fig. 5F**; LA: from 0.43 ± 0.05 Hz

343 to 0.43 ± 0.06 Hz, n = 8, N = 5, $P > 0.05$, **Fig. 5H**). While the above results were
344 observed in the male mice, similar results were observed in the female mice (**sFig.8 A**
345 and **B**).
346 Consequence of knocking down TRPC6 described above should not be a result of a
347 secondary effect on other TRPC channels with which TRPC6 is known to interact to
348 form heteromers, such as TRPC4 and TRPC7[47, 48], since in experiments using
349 single cell PCR (**sFig. 9A**), it was found only a very small proportion of
350 TRPC6-positive DA cells (DAT^+) expressed TRPC4 (**sFig. 9Bi**) or TRPC7 (**sFig.**
351 **9Bii**), in consistent with the results of single-cell RNA-seq results (**Fig. 2**).
352 Taken together, above results indicate TRPC6 is an important contributor in
353 subthreshold depolarization and spontaneous firing of the VTA DA neurons.
354
355 **Down-regulation of TRPC6 contributes to the altered firing activity of the VTA**
356 **DA neurons in depression model**
357 In multiple depression models, the depression-like behavior was directly linked to the
358 altered firing activity of the VTA DA neurons[4, 7, 49-51]. In consideration of the
359 evidence we described above that NALCN and TRPC6 play key roles in firing
360 activity of the VTA DA neurons, we went further to study if these channels also
361 contributed to the altered firing activity of the VTA DA neurons and to the
362 development of the depression-like behavior in depression models of mice.
363 We first established a mice depression model of chronic mild unpredictable stress
364 (CMUS) [52], which, after 5 weeks subjecting to two different stressors every day
365 (**Fig. 6A**), manifested chronic-stress-induced depression-like behaviors in the sucrose
366 preference test (SPT) and the tail suspension test (TST), with reduced sucrose
367 preference and lengthened immobility time, respectively (**Fig. 6B**). Multiple other
368 behaviors tests were also performed on these CMUS mice (**sFig. 10**), all indicating
369 depression/anxiety-like behaviors.
370 It has been shown that a reduced firing activity in the VTA DA neurons is responsible
371 for the chronic-stress-induced depression-like behavior in the CMUS model[51, 53].
372 Consistent with this finding, we also found the firing frequency of the VTA DA
373 neurons from the CMUS male mice was significantly reduced as compared with that

374 from the control male mice (2.83 ± 0.42 Hz, n = 18, N = 5 for control mice *vs* 1.30 ±
375 0.14 Hz, n = 28, N = 5 for CMUS mice, $P < 0.01$, **Fig. 6C**). In agreement with a role
376 for TRPC6 in this reduced firing activity, TRPC6 protein in the male VTA tissue was
377 found to be down-regulated in western blot experiments (**Fig. 6D**). On the other hand,
378 NALCN protein in the VTA was not altered in the CMUS male mice model of
379 depression (**sFig. 11**).
380 We also tested if this down-regulation of TRPC6 protein could also be found in a
381 similar but different model of depression. For this, a chronic restraint stress (CRS)
382 model was used. After 3 weeks of restraint stress stimulation, the CRS male mice
383 developed similar depression/anxiety-like behavior in the behavior tests like these
384 similarly performed in the CMUS model (**sFig. 12A-I**). Importantly, male mice with
385 CRS-induced depression also showed a significant downregulation of TRPC6 protein
386 in the VTA (0.43 ± 0.09 fold, N = 6 for control and N = 9 for CRS, $P < 0.001$, **sFig.**
387 **12J**). In female CMUS mice (**sFig13. A-I**), TRPC6 protein in the VTA tissue was also
388 found to be down-regulated in western blot experiments (**sFig. 13J**).
389 It is known that CMUS mainly decreases the activity of VTA dopamine neurons that
390 project to mPFC[11, 51]. Assuming that the decreased firing activity of the
391 mPFC-projecting VTA DA neurons in the CMUS mice was associated with the
392 down-regulation of TRPC6 expression, we reasoned that the firing activity in these
393 CMUS mice would respond less to the TRP channel inhibitors. Indeed, TRP channel
394 inhibitor 2-APB and TRPC6 inhibitor LA decreased their inhibitory effect on the
395 firing activity of the mPFC-projecting VTA DA neurons from the CMUS male mice
396 (2-APB: 1.61 ± 0.23 Hz to 1.19 ± 0.22 Hz, n = 15, N=5, $P > 0.05$; LA: 0.97 ± 0.15 Hz
397 to 0.66 ± 0.09 Hz, n = 19, N = 8, $P > 0.05$) compared with these from the control male
398 mice (2-APB: 3.74 ± 0.42 Hz to 0.17 ± 0.09 Hz, n = 12, N = 5, $P < 0.001$; LA: 2.83 ±
399 0.17 Hz to 0.10 ± 0.07 Hz, n = 17, N = 8, $P < 0.001$) (**Fig. 6E** and **F**).
400 Taken together, above results suggest down-regulation of TRPC6 is a key determinant
401 for the altered firing activity of the VTA DA neuron in mice models of depression
402
403 **Down-regulation of TRPC6 in the VTA DA neurons confer the mice with**
404 **depression-like behavior**

405 If down-regulation of TRPC6 is crucial for the depression-like behaviors, like that
406 indicated above in the CMUS and the CRS depression models, then down regulation
407 of TRPC6 in non-stressfully treated mice should also develop depression-like
408 behavior. We tested this possibility by selectively knocking down TRPC6 in the VTA
409 DA neurons, using DAT-Cre male mice injected with a AAV viral construct
410 (AAV9-hSyn-DIO-shRNA (TRPC6) -RFP) (**Fig. 7A**), driving the expression of
411 shRNA against TRPC6 selectively in the VTA DA neurons. Three weeks after the
412 AAV injection, the qPCR (**Fig. 7B**) and the immunofluorescence results (**Fig. 7C**)
413 indicated an efficient down-regulation of TRPC6 in the VTA DA neurons.
414 We next compared the depression- and anxiety-like behaviors in these conditionally
415 TRPC6-knockout male mice (TRPC-cKD) with that in the control mice (infected with
416 virus carrying the scrambled shRNA). As shown in **Fig. 7D**, in the TRPC6-cKD mice,
417 the sucrose preference was significantly reduced (7Di, 72.60 ± 3.52%, N = 13 for
418 TRPC6-cKD, *vs* 92.74 ± 0.86 %, N = 9 for control, $P < 0.001$), the immobility time in
419 the TST was significantly lengthened (7Dii, 192.10 ± 3.13 s *vs* 133.20 ± 8.89 s, $P <$
420 0.001). In the elevated plus maze test, the percentage of time spent in the open arm
421 was significantly reduced (7Diii, 2.43 ± 0.48 % *vs* 14.78 ± 1.26 %, $P < 0.001$) and the
422 percentage of time spent in the closed arm was also significantly increased (7Div).
423 And the Cre-dependent TRPC6-overexpression in male VTA DAT-Cre mice
424 (TRPC6-cOE) rescued the selective-TRPC6-knockdown-induced depression-like
425 behaviors (**Fig. 7E-H**). Furthermore, selectively knockdown of TRPC6 in the
426 mPFC-projecting VTA DA neurons (virus-retro carrying DIO-TRPC6-shRNA
427 (TRPC6-rcKD) was injected into the mPFC of DAT-Cre male mice) (**Fig. 8A-C**) also
428 conferred the mice with the depression- and anxiety-like behaviors (**Fig. 8D**).
429 Taken together, these results suggest downregulation of TRPC6 in the VTA DA
430 neurons confers the mice with phenotypes of depression/anxiety.
431

432 ## Discussion

433 In this study, we made a systematic study on the molecular mechanism for the
434 subthreshold depolarization that drive spontaneous firing of the VTA DA neurons. We
435 identified TRPC6 channels, alongside NALCN, as major contributors to this

436 subthreshold depolarization and related spontaneous firing, and further importantly,
437 we also demonstrated that TRPC6 contributed to the altered firing activity of the VTA
438 DA neurons under states of chronic-stress-induced depression-like behaviors.
439 The nature of a relatively depolarized resting membrane potential in the VTA DA
440 neurons imposes a need for a full understanding of the channel conductance
441 underlying this depolarization. It is first clear from these current and previous studies
442 that this conductance is mediated by a persistent Na^+ influx. Unlike the DA neurons in
443 the SNc, where Ca^{2+} influx is needed for the spontaneous firing [54], the results in our
444 and others' studies indicate Ca^{2+} influx are not necessary for the spontaneous firing of
445 the VTA DA neurons, rather, replacement of Ca^{2+} ions in the extracellular fluid with
446 Mg^{2+} accelerates the frequency of spontaneous firing (Fig. 1B) [15], possibly due to a
447 reduced activity of the Ca^{2+}-activated K^+ currents and the increased activity of
448 NALCN[28, 55]. Consistent with these finding and more precisely for a role of Ca^{2+}
449 influx on the subthreshold depolarization, removing extracellular Ca^{2+} did not
450 hyperpolarize the RMP. On the other hand, consistent the previous study [15], a
451 TTX-insensitive Na^+ influx clearly contributed to the subthreshold depolarization (Fig.
452 1D).
453 A TTX-insensitive nature of this Na^+ conductance suggests that cation conductance
454 permeable to Na^+ might be the molecular candidates. We first focused on the HCN
455 channels because, (1) it has been suggested HCN channels are important regulators
456 for the spontaneous firing of VTA DA neurons under states of depression-like
457 behaviors[7, 11]; (2) HCN are one of the more highly expressed NSCCs in the VTA
458 DA neurons in our single cell RNA-Seq study; (3) HCN are permeable to Na^+[56].
459 However, it is clear from our study that HCN does not contribute to the spontaneous
460 firing of the VTA DA neurons in the adult mice; none of the known HCN blockers we
461 used had any significant effects on the firing activity. Presence of HCN has long been
462 used as a signature of DA neurons[57], also as a differentiating factor for the
463 projection-specificity of the VTA DA neurons[39]. Nonetheless, contribution of HCN
464 to the spontaneous firing of the VTA DA neurons has been controversial; the HCN
465 blockers ZD7288 and CsCl have been reported as both effective[23, 24, 58] and

466 non-effective [15] on the spontaneous firing of the VTA DA neurons. A closer
467 inspection into our and others' results present a possible explanation for these
468 different results: in the younger rodents (less than one month old) (sFig.5) [59], the
469 HCN in the DA neurons play a more important role whereas in the adult mice (~ 8
470 weeks)[59], like the ones we used in this study, the HCN do not contribute to the
471 spontaneous firing of the VTA DA neurons. This is likely due to a shift of activation
472 gating of HCN channels in a hyperpolarization direction with age, thus the
473 modulation of HCN on the firing activity diminishes with age, as it is described in the
474 SNc DA neurons[59]. Consistent with this, we found hyperpolarizing the RMP
475 rendered the VTA DA neurons of the adult mice with sensitivity to the HCN blockers.
476 Thus, the VTA DA neurons in adult mice do not use HCN to depolarize the membrane
477 to generate action potentials.
478 NALCN is widely expressed in central neurons[60, 61], and is a popular candidate
479 considered for the ion mechanism of the subthreshold depolarization currents and Na^+
480 leaky currents. NALCN has been shown to be an important component of background
481 Na^+ currents and to be important for neuronal excitability in the hippocampal neurons,
482 posterior rhomboid nucleus (Retrotrapezoid nucleus/RTN)) chemo-sensitive neurons
483 (CO_2/H^+-sensitive neurons), GABA neurons and DA neurons in the substantia nigra,
484 and spinal projection neurons [26, 28-31, 42]. Our results with single cell RNA-Seq
485 and immunofluorescence methods validated high level expression of NALCN in the
486 VTA DA neurons; both the pharmacological and the NALCN-gene-knockout
487 experiments demonstrated convincingly involvement of NALCN in subthreshold
488 depolarization and spontaneous firing of the VTA DA neurons.
489 We did not detect alteration of NALCN protein expression in the depression model of
490 CMUS in the VTA tissue. However, this does not completely exclude a possible
491 contribution of NALCN to the altered functional activity of the VTA DA neurons
492 which underlies the chronic-stress-induced depression-like behaviors. Future study
493 focusing on the functional property of NALCN in the cellular level of the VTA DA
494 neurons under a state of depression is needed to clarify this issue. NALCN is after all
495 a potential drug target in consideration of its important contribution to the resting

496 membrane potential and functional activity of neurons.

497 The most interesting and important finding of this study is the role of TRPC6 in
498 regulation of the firing activity of the VTA DA neurons in both physiological and
499 depression-state conditions, and its involvement in depression-like behaviors; the
500 experimental evidence from pharmacological, gene silencing, electrophysiological
501 and behavior results unambiguously support this conclusion. It is interesting to note,
502 although with an unclear neuronal circuit mechanism of action, the TRPC6 channel
503 opener hyperforin was previously reported to have antidepressant effects in
504 corticosterone-depressed mice, which were reversed by prior administration of the
505 TRPC6 blocker larixyl acetate[62]. Also, in a CMUS rat model, TRPC6 expression
506 was found to be downregulated in the hippocampus, and administration of the TRPC6
507 opener hyperforin was effective in alleviating depression-like behavior[63]. Our study
508 provides strong and convincing evidence that TRPC6 is a key regulator of the VTA
509 DA neurons which are known to be a key player in depression states [7, 21, 49, 50,
510 64].

511 The above-mentioned role for TRPC6 should come from its contribution to the
512 subthreshold depolarization, through a persistent permeation to the influx of Na^+.
513 Although TRPC channels has been better recognized for their permeability to Ca^{2+}
514 and their regulation on cellular Ca^{2+} homeostasis, the importance of TRPC channels
515 for the permeability of monovalent cations, especially Na^+, is now gradually being
516 appreciated [65]. In the substantial nigra GABA and DA neurons, TRPC3 has been
517 reported to play an important role in maintaining depolarization membrane potential,
518 pacemaking, and firing regularity[31, 33]. Otherwise, it has been reported that slow
519 tonic firing of SNc DA neurons, depends on the basal activity of both the NALCN and
520 TRPC3 channels, but that burst firing does not require TRPC3 channels but relies
521 only on NALCN channels[66]. TRPC6 and TRPC3 belong to the same TRPC family
522 subclass and TRPC6 is more than 75% homologous to TRPC3[45]. Interestingly, our
523 results with single-cell RNA-Seq and single-cell PCR demonstrated the rich
524 expression of TRPC6 in the VTA DA neurons among all TRP channels but no
525 expression of TRPC3 was found in these neurons. These results present an

526 opportunity for selectively targeting a single TRPC channel to exert selective
527 pharmacological results. Besides, TRPC4 expression was detected in a uniformly
528 distributed subset of VTA DA neurons[35], which is consistent with our results with
529 single-cell RNA-Seq, and TRPC4 KO rats showed decreased VTA DA neuron tonic
530 firing and deficits in cocaine reward and social behaviors[35].

531 It has also been demonstrated in cell types other than neurons, such as rat portal vein
532 smooth muscle cells, the activation of α-adrenergic receptor can open TRPC6, which
533 leads to cell depolarization, activation of voltage-dependent Ca^{2+} channels, and
534 ultimately the contraction of smooth muscle cell[67]; it is also shown that angiotensin
535 II and endothelin I can activate TRPC3/C6 heterodimers via vascular G
536 protein-coupled receptors (GPCR), thereby depolarizing cells [68, 69]. Following this
537 line, it would be very interesting to know if TRPC6 in the VTA DA neurons, where
538 multiple GPCR reside receiving input and auto modulation by neuronal transmitters
539 [70, 71], could also be a target of modulation with similar mechanism. In
540 consideration of the important role, we described here in this study, this type of
541 modulation will present possible explanations for some unsolved mechanism for
542 physiological and pathophysiological functions of the VTA DA neurons.

543 The facts that down-regulation of TRPC6 proteins was correlated with reduced firing
544 activity of the VTA DA neurons, the chronic-stress-induced depression-like behaviors,
545 and that knocking down of TRPC6 in the VTA DA neurons confers the mice with
546 depression-like behaviors strongly suggest a crucial role for TRPC6 in the
547 development of chronic-stress-induced depression-like behaviors under stressful
548 conditions like CMUS. To reinforce this, down-regulation of TRPC6 was also found
549 in another chronic-stress-induced depression model of CRS, a model with similar
550 neuronal alteration of reduced firing activity in the VTA DA neurons to that described
551 in the CMUS model[72]. These facts with the fact that TRPC6 activator hyperforin is
552 an effective antidepressant in multiple depression models[62, 63], and that hyperforin
553 is the principal component of St. John's wort, a well-known antidepressant herb[73],
554 present TRPC6 as a very attractive drug target for new lines of antidepressants.

555 **Materials and methods**

556 **Animal Preparation**

557 Male or female 6-8-week-old C57BL/6 (Vital River, China) and DAT-Cre mice with a
558 C57BL/6 background (Stock No: 006660, the Jackson Laboratories, USA) were used
559 for the studies. All experiments were conducted in accordance with the guidelines of
560 Animal Care and Use Committee of Hebei Medical University and approved by the
561 Animal Ethics Committee of Hebei Medical University.

562 **Brain slice preparation**

563 The details for the preparation of coronal brain slice containing VTA were the same as
564 described in our previously published work[21, 70]. Briefly, mice were anesthetized
565 with chloral hydrate (200 mg/kg, i.p.). After intracardial perfusion with ice-cold
566 sucrose solution, the brains of the mice were removed quickly and placed into the
567 slicing solution. The ice-cold sucrose-cutting solution contained (in mM): sucrose 260,
568 $NaHCO_3$ 25, KCl 2.5, NaH_2PO_4 1.25, $CaCl_2$ 2, $MgCl_2$ 2, and D-glucose 10;
569 osmolarity, 295-305 mOsm). Using the vibratome (VT1200S; Leica, Germany), the
570 coronal midbrain slices (250 μm-thick) containing VTA were sectioned. The slices
571 were incubated for 30 min at 36°C in oxygenated artificial cerebrospinal fluid (ACSF)
572 (in mM: NaCl 130, $MgCl_2$ 2, KCl 3, NaH_2PO_4-$2H_2O$ 1.25, $CaCl_2$ 2, D-Glucose 10,
573 $NaHCO_3$ 26; osmolarity, 280-300 mOsm), and were then left for recovery for 60 min
574 at room temperature (23-25°C) until use.
575 The brain slices were transferred to the recording chamber and were continuously
576 perfused with fully oxygenated ASCF during recording.

577 **Identification of DA neurons and electrophysiological recordings**

578 Recordings in the slices were performed in whole-cell current-clamp and
579 voltage-clamp configurations on the Axoclamp 700B preamplifier (Molecular Devices,
580 USA) coupled with a Digidata 1550B AD converter (Molecular Devices, USA).
581 Neurons in the VTA were visualized with a 40X water-immersion objective equipped
582 by an optiMOS microscope camera (Qimaging, Canada) on an Olympus-BX51
583 microscope (Olympus, Japan). Projection-specific or GFP-positiveVTA neurons were
584 identified by infrared-differential interference contrast (IR-DIC) video microscopy

585 and epifluorescence (Olympus, Japan) for detection of retrobeads (red) positive or
586 GFP-positive neurons.
587 For whole-cell recording, glass electrodes (3-5 MΩ) were filled with internal solution
588 (in mM): K-methylsulfate 115, KCl 20, $MgCl_2$ 1, HEPES 10, EGTA 0.1, MgATP 2
589 and Na_2GTP 0.3, pH adjusted to 7.4 with KOH. And the extracellular solution was the
590 ACSF.
591 In whole-cell current-clamp mode, HCN function was judged by the inwardly
592 rectifying characteristic sag potential generated by giving a hyperpolarizing current
593 (-100 pA).
594 When recording the effect of removing extracellular Ca^{2+} on spontaneous cell
595 discharge, $CaCl_2$ in the ACSF was replaced with $MgCl_2$, and the final $MgCl_2$
596 concentration was 4 mM.
597 The resting membrane potential (RMP) was measured in current clamp mode (I = 0);
598 the composition of the recording solution (mM) contained: NaCl 151, KCl 3.5, $CaCl_2$
599 2, $MgCl_2$ 1, glucose 10, and HEPES 10, and the pH was adjusted to about 7.35 with
600 NaOH. 1 μM tetrodotoxin was added to the extracellular solution to abolish action
601 potential during measurement of the RMP.
602 To observe the effect of extracellular Na^+ on the RMP, NaCl in the original recording
603 solution was replaced with equimolar NMDG, and the NMDG-recording solution
604 (mM) contained: NMDG 151, KCl 3.5, $CaCl_2$ 2, $MgCl_2$ 1, glucose 10, and HEPES 10,
605 and the pH was adjusted to 7.35 with KOH.
606 For recording spontaneous firing of the neurons, cell-attached "loose-patch" (100-300
607 MΩ) recordings were used[74]. In this case, patch-pipettes (2-4 MΩ) were filled with
608 ACSF, and the spontaneous activity was recorded in the current-clamp mode (I = 0).
609 The synaptic blockers (CNQX, 10 μM; APV, 50 μM and gabazine, 10 μM) were
610 added to isolate the intrinsic firing properties.
611 At the end of electrophysiological recordings, the recorded VTA neurons were
612 collected for single-cell PCR.VTA DA neurons were identified by single-cell PCR for
613 the presence of TH and DAT.
614
615 **Retrograde labelling**

616 Briefly, under general chloral hydrate anaesthesia (200 mg/kg, i.p.) and stereotactic
617 control (RWD Instruments, Guangzhou, China), the skull surface was exposed. All
618 coordinates are relative to bregma in mm using landmarks and neuroanatomical
619 nomenclature that was described in the Franklin and Paxinos mouse brain atlas[75] .
620 Red retrobeads (100 nl for single injection; Lumafluor Inc., Naples, FL, USA) were
621 injected into the following sites using KD scientific syringe pump (KD scientific,
622 Holliston MA, USA): bilaterally into NAc core (NAc c), NAc lateral shell (NAc ls),
623 NAc medial shell (NAc ms) and basolateral amygdala (BLA), 4 separate sites (2 per
624 hemisphere) into medial prefrontal cortex (mPFC). Coordinates for infusions were as
625 follows: NAc c (AP +1.50, LM 0.84, DV -4.0; 100 nl beads); NAc ls (AP +0.86, LM
626 1.72, DV -4.0; 100 nl beads); NAc ms (AP +1.70, LM 0.53, DV -4.0; 100 nl beads);
627 mPFC (AP +2.05 and 2.15, LM 0.27, DV -2.1 + 1.7; 200 nl beads); BLA (AP -1.46,
628 LM 2.85, DV -4.3; 100 nl beads). Retrobeads were delivered through a pulled glass
629 pipette using a PAP107 Multipipette Puller (MicroData Instrument, Inc., USA) and at
630 a rate of 100 nl/min; the injection needle was left in place for at least 5 minutes after
631 each infusion. Following surgery, mice were returned to single housing. For sufficient
632 labelling, survival periods for retrograde tracer transport depended on respective
633 injection areas: NAc c, NAc ls, NAc ms, 14 days; mPFC, 21 days; BLA 14 days[39].
634 Coronal sections of injection sites were stained with 4, 6-diamidino-2-phenylindole
635 (DAPI, Sigma, USA) to confirm representative target location. Then, serial analyses
636 of the injection-sites were carried out routinely.
637
638 **AAV for gene knockdown or overexpression and viral construct and injection**
639 For knockdown of NALCN and TRPC6, AAV9-U6-shRNA (NALCN)-CMV-GFP
640 (300 nl) or AAV9-U6-shRNA (TRPC6)-CMV-GFP or its control
641 AAV9-scramble-shRNA was delivered into the VTA (AP, −3.08 mm; ML, ±0.50 mm;
642 DV, −4. 50 mm) of the mice. AAV9-hSyn-DIO-shRNA (TRPC6)-RFP (300 nl) or its
643 control AAV9-scramble-shRNA was delivered into the VTA of the DAT-Cre C57BL/6
644 mice. AAV-retro-hSyn-DIO-mCherry-shRNA (TRPC6) (300 nl) or its control
645 AAV-retro-scramble-shRNA was delivered into the mPFC of the DAT-Cre C57BL/6
646 mice.

The shRNA hairpin sequences used in this study:

NALCN shRNA: AAGATCGCACAGCCTCTTCAT[26];

TRPC6 shRNA: 5'-CCAGGATCAATGCATACAA-3'.

For Cre-dependent overexpression of TRPC6, AAV9-DIO-TRPC6-GFP (300 nl) or its control AAV9-scramble-RNA was delivered into the VTA of the DAT-Cre C57BL/6 mice, 7 days after injection of AAV9-hSyn-DIO-shRNA (TRPC6)-RFP.

Mice were singly housed with enough food and water to recover for 4-5 weeks after injection of virus, before behavior tests and electrophysiological recordings.

Single cell PCR

mRNA was reversely transcribed to cDNA by PrimeScript^{TM}II1st Strand cDNA Synthesis Kit (Takara-Clontech, Kyoto, Japan). At the end of electrophysiological recordings, the recorded neuron was aspirated into a pipette and then expelled into a PCR sterile tube containing 1 μl oligo-dT Primer and 1 μl dNTP mixture. The mixture was heated to 65°C for 5 min to denature the nucleic acids and then cooled on ice for 2 min. Reverse transcription from mRNA into cDNA was performed at 50°C for 50 min and then 85°C for 5 sec. cDNA was stored at -40°C. Then two rounds of conventional PCR with pairs of gene-specific outside (first round) and inner primers (second round) for GAPDH (positive control), TH, DAT, D2, GIRK2, Vgult2, GAD1, NALCN, TRPC6, TRPV2 and TRPC3 using GoTaq Green Master Mix (Promega, Madison, USA) were performed. After adding the specific outside primer pairs into each PCR tube, first-round synthesis conditions were as follows: 95 °C (5 min); 30 cycles of 95 °C (50 s), 58-63 °C (50 s), 72 °C (50 s); 72 °C(5 min). Then, the product of the first PCR was added in the second amplification round by using specific inner primer (final volume 25 μl). The second amplification round consisted of the following: 95 °C (5 min); 35 cycles of 95 °C (50 s), 58 °C-62 °C (45 s), 72 °C (50 s) and 5 min elongation at 72 °C. The final PCR products were separated by electrophoresis on 2% agarose gels. The negative control reactions with no added template were also performed in each experiment.

The “outer” primers (from 5′ to 3′) as follows:

GAPDH:

AAATGGTGAAGGTCGGTGTGAACG（sense）

AGTGATGGCATGGACTGTGGTCAT （antisense）

TH:

GCCGTCTCAGAGCAGGATAC

GGGTAGCATAGAGGCCCTTC

DAT:

CTGCCCTGTCCTGAAAGGTGT

GCCCAGTGATCACAGACTCC

D2-R:

AGCATCGACAGGTACACAGC

CCATTCTCCGCCTGTTCACT

GIRK2:

TGGACCAGGATGTGGAAAGC

AAACCCGTTGAGGTTGGTGA

Vgult2:

CTGCTTCTGGTTGTTGGCTACTCT

ATCTCGGTCCTTATAGGTGTACGC

GAD1:

ACAACCTTTGGCTGCATGTGGATG

AATCCCACGGTGCCCTTTGCTTTC

NALCN:

TCCATCTGTGGGAAGCATGT

CAAAAGCTGGTCCTCTTCAGTG

TRPC6:

AGCCTGTCTATTGAGGAAGAAC

AGCGAGAATGATTGGGGTCA

TRPV2:

CTGCACATCGCCATAGAGAA

AGGCTGGTGGTAGGCAACTA

TRPC3:

GCTGGCCAACATAGAGAAGG

CCTGCACGTGACTATCCACA

709 TRPC4:

710 GTCTATGTAGGCGATGCGCT

711 AGGAGGTCCTTGGCAAATTGT

712 TRPC7:

713 GCCATCAGCAAGGGCTATGT

714 CACGCCCACCACAAAATCC

715 The “inner” primers (from 5′ to 3′) as follows:

716 GAPDH:

717 GCAAATTCAACGGCACAGTCAAGG

718 TCTCGTGGTTCACACCCATCACAA

719 TH:

720 AGGAGAGGGATGGAAATGCT

721 ACCAGGGAACCTTGTCCTCT

722 DAT:

723 ATTTTGAGCGTGGTGTGCTG

724 TGCCTCACAGAGACGGTAGA

725 D2-R:

726 CCATTGTCTGGGTCCTGTCC

727 GTGGGTACAGTTGCCCTTGA

728 GIRK2:

729 AGCCGAGACAGGACCAAAAG

730 ATGTACGCAATCAGCCACCA

731 Vgult2:

732 CATCTCCTTCTTGGTGCTTGCAGT

733 ACAGCGTGCCAACGCCATTTGAAA

734 GAD1:

735 AGTCACCTGGAACCCTC

736 GCTTGTCTGGCTGGAA

737 NALCN:

738 GCCTTTGCTGGAGTTGTTCTG

739 CCCTGCATAATTGCCACAGTC

740 TRPC6:
741 TGCTAGAAGAGTGTCATTCCCT
742 CCTCCACAATCCGTACATAACC
743 TRPV2:
744 GTGGGATGTGGTGACCTACC
745 GCTGGTACAGCCCTGAGAAC
746 TRPC3:
747 CCTTGGGTCTTCCATTCCTC
748 CACAACTGCACGATGTACTCC
749 TRPC4:
750 CCACGAGGTCCGCTGTAAC
751 CTCCCAACTTAACTGAAAGGCA
752 TRPC7:
753 CGCTTCTCCCACGACATCAC
754 ACTGGATAGGGACAGGTAGGC
755 **RT-qPCR**
756 Total RNA was prepared using Trizol. RNA was reversely transcribed into cDNA by
757 TAKARA PrimeScripttm RT reagent Kit with gDNA Eraser for Reverse transcription.
758 Subsequently, the SYBR Green Master Mix (TaKaRa) was used to do the qRT-PCR
759 assays.
760 The specific primers were:
761 GAPDH：
762 GCAAATTCAACGGCACAGTCAAGG
763 TCTCGTGGTTCACACCCATCACAA
764 TRPC6：
765 GCAGAAACACAGAGGAAGTGG
766 GCTCTTTCCAGCTTGGCATATC
767 NALCN：
768 TAATGAGATAGGCACGAGTA
769 TGATGAAGTAGAAGTAGGAG
770

Single cell RT-qPCR

Following the retrograde labelling and VTA brain slice preparation, projection-specific VTA neurons were identified by infrared-differential interference contrast (IR-DIC) video microscopy and epifluorescence (Olympus, Japan) for detection of retrobeads (red) positive neurons. mRNA was reversely transcribed to cDNA by PrimeScript^{TM}II1st Strand cDNA Synthesis Kit (Takara-Clontech, Kyoto, Japan). The projection-specific neurons was aspirated into a pipette and then expelled into a PCR sterile tube containing 1 μl oligo-dT Primer and 1 μl dNTP mixture. The mixture was heated to 65°C for 5 min to denature the nucleic acids and then cooled on ice for 2 min. Reverse transcription from mRNA into cDNA was performed at 50°C for 50 min and then 85°C for 5 sec. cDNA was stored at -40°C. The targeted pre-amplification was done, with pairs of targeted primers for GAPDH, TH and TRPC6, to quantify multiple targets per cell. After adding the targeted primer pairs into each PCR tube, the synthesis conditions were as follows: 95 °C (5 min); 10 cycles of 95 °C (50 s), 58-62 °C (50 s), 72 °C (50 s); 72 °C (5 min). After targeted pre-amplification, Quantitative PCR (qPCR) is the final laboratory step of the scRT-qPCR workflow with the SYBR Green Master Mix (TaKaRa).

The targeted primers for pre-amplification (from 5′to 3′) as follows:

GAPDH:

AAATGGTGAAGGTCGGTGTGAACG（sense）

AGTGATGGCATGGACTGTGGTCAT （antisense）

TH:

AAGGTTCATTGGACGGCGG

ACATCGTCAGACACCCGAC

TRPC6:

AGCCTGTCTATTGAGGAAGAAC

AGCGAGAATGATTGGGGTCA

The primers for qPCR (from 5′ to 3′) as follows:

GAPDH:

GCAAATTCAACGGCACAGTCAAGG

TCTCGTGGTTCACACCCATCACAA

802 TH:
803 TCTCCTTGAGGGGTACAAAACC
804 ACCTCGAAGCGCACAAAGT
805 TRPC6:
806 TGCTAGAAGAGTGTCATTCCCT
807 CCTCCACAATCCGTACATAACC
808
809 **Immunofluorescence**
810 After intracardial perfusion with 4% paraformaldehyde (PFA) in 0.01 M PBS (pH 7.4).
811 The brains were post-fixed in 4% paraformaldehyde. 48 h later, the brain tissue was
812 placed in 30% sucrose solution (PBS preparation) to dehydrate. The brain tissue was
813 sectioned coronally, including the nucleus accumbens (NAc), medial prefrontal cortex
814 (mPFC), basolateral amygdala (BLA), and VTA, using a vibrating microtome. The
815 section thickness of NAc, mPFC and BLA was 80μm and the section thickness of
816 VTA was 40 μm. The sections were placed in PBS solution and stored in a
817 refrigerator at 4°C for storage.
818 The brain section was incubated in 0.3% triton/3% BSA for 1 h at room temperature
819 and then was blocked with 10% donkey serum at 37°C for 1 h. After that, the brain
820 section was incubated in the corresponding antibodies in PBS at 4°C for 24 h. The
821 section was washed three times (10 min) with PBS. Finally, the brain section was
822 incubated in the secondary antibodies for 2 h at 37°C. Images were obtained on a
823 Leica TCS SP5 confocal laser microscope (Leica, Germany) equipped with laser lines
824 for 405 mm, 488 mm, 561 mm and 647 mm illumination. Images were analyzed with
825 LAS-AF-Lite software (Leica, Germany).
826
827 **Single-cell whole-transcriptome gene sequencing**
828 After retrobeads injection, following brain slice preparation and 1 h recording, the
829 recorded and retrobeads-labelled neurons were aspirated into the patch pipette and
830 were then broken into the PCR tube containing 1 μl lysis buffer. For mRNA in
831 individual cells, mRNA was amplified and cDNA by SMARTer Ultra Low Input RNA
832 for Illumina Kit, which was qualified and reversely transcribed to cDNA by Qubit and

833 Agilent Bioanalyzer 2100 electrophoresis. After fragmentation of cDNA (300 bp) by
834 ultrasound, sequencing libraries (end repair, addition of poly(A), and ligation of
835 sequencing connectors) were built using the Ovation Ultralow Library System V2.
836 After that, the constructed libraries were sequenced using Illumina HiseqXten
837 (Sinotech Genomics Co., Ltd.).
838
839 **Depression models**
840 Chronic Mild Unpredictable Stress (CMUS) procedure
841 The CMUS procedures consisted of food and water deprivation (24 h), day/night
842 inversion, damp bedding (12 h), cage tilt (12 h), no bedding (12 h), rat bedding (12 h),
843 4°C cold bath (5 min), restraint (2 h)and tail pinching (30 min). Mice were subjected
844 to consecutive 35 days of CMUS with two stressors per day. Non-stressed controls
845 were handled only for cage changes and behavioral tests.
846 Chronic Restraint Stress (CRS) procedure
847 The mice were immobilized in a special restraint device for 6 h per day from 9:00 to
848 15:00 for 21 days.
849 Behavior tests
850 The behavior tests were performed in the following order.
851 Sucrose preference test
852 Mice were single-housed and trained to drink from two drinking bottles with 1 bottle
853 of tap water and 1 bottle of 1% sucrose water, for 48 hours, and the positions of the
854 drinking bottles were exchanged every 12 h to exclude the interference of position
855 preference. After the training, the mice were deprived of food and water for 12 h, and
856 then the sucrose preference test was performed for 24 h. One bottle of tap water and
857 one bottle of 1.0 % sucrose water were given again, and the positions of the drinking
858 bottles were exchanged at 12 h. Finally, the consumption of tap water and sugar water
859 at 24 h were recorded to calculate the sucrose solution preference rate. Sucrose
860 preference rate = sucrose solution consumption/(tap water consumption + sucrose
861 solution consumption).
862 Open field test, OFT
863 The mice were placed in a topless chamber (40 cm × 40 cm × 30 cm) with a camera

mounted on top of the chamber and connected to ANY-maze video tracking system on the computer to automatically track and record the activity of mice during the experiment and to obtain behavioral data. The bottom of the chamber was divided into 16 small square grids (10 cm × 10 cm) on the computer, and four square grids in the central area were defined as the central zone. During the 10 min test session, Total distance traveled and time spent in the center were recorded.

Elevated plus maze, EPM

The EPM apparatus consists of two closed arms (25 x 5 cm) across from each other and perpendicular to two open arms (25 x 5 cm) that are connected by a center platform (5 x 5 cm), with a camera in the center ceiling to automatically track and record the activity of mice. Mice were placed in the center platform facing a closed arm and allowed to freely explore the maze for 7 min, of which the first 2 min was the adaptation time. The time spent in open arms was analyzed for last 5 min after the adaptation.

Accelerating rotarod test

Locomotor activity was estimated by accelerating the rotarod test. Each group of animals was placed on an accelerating rotarod walking for 300 s from 4 to 40 rpm. After three days of training (three times per day), latency was automatically recorded from the beginning of the trial until the mouse falls off.

Forced swimming test, FST

Forced swimming test (FST) was performed in a glass cylinders, filled with the water depth about 15 cm at room temperature. The experiment was conducted for 5 min, of which the first 1 min was the adaptation time and the mice were allowed to move freely, and the immobility time was recorded for last 4 min after the adaptation.

Tail suspension test, TST

Mouse was suspended by taping the tail (1 cm from the tip of the tail) to the fixation device for 6 min. The cumulative immobility time within last 4 min was recorded, and the time when all limbs were immobile except for respiration was considered as immobility time.

Western Blot

895 The VTA protein was isolated by100 μl RIPA and 1 μl PMSF. The total protein for
896 each sample was transferred onto the polyvinylidene difluoride (PVDF) membranes
897 after SDS-polyacrylamide gel electrophoresis (SDS-PAGE), and blocked 2 h at room
898 temperature with 5% bovine serum albumin (KeyGen Biotechnology). Subsequently,
899 all these membranes were incubated overnight at 4 °C with the primary antibodies as
900 below: TRPC6, NALCN, and GAPDH. Following 2 h secondary antibodies
901 incubation, all the bands were detected. The relative expression was calculated based
902 on the internal control GAPDH.
903
904 **Drugs and reagents**
905 Drugs were bath applied at the following concentrations:
906 6-cyano-7-nitroquinoxaline-2,3-dione (CNQX; 10 μM; Sigma),
907 DL-2-amino-5-phosphonopentanoic acid (APV; 50 μM; Sigma) and gabazine (10 μM;
908 Sigma), CsCl (3 mM; sigma), ZD7288 (60 μm; Abcam), TTX (1 μM; MCE), $GdCl_3$
909 (100 μM; Sigma), L703,606 (10 μM; Sigma), 2-Aminoethyldiphenylborinate (2-APB,
910 100 μM; Sigma), Larixyl acetate (10 μM; Sigma), Ruthenium Red (60 μM; TCI).
911 Commercial antibodies used were: Anti-Tyrosine Hydroxylase Antibody (1:400,
912 Millipore, MAB318, RRID: AB_2201528, for Immunofluorescence), Anti-Dopamine
913 Transporter (N-terminal) antibody (1:400, sigma, D6944, RRID: AB_1840807, for
914 Immunofluorescence), Anti-NALCN (1:100, Thermo Fisher Scientific, MA5-27593,
915 RRID: AB_2735285, for Immunofluorescence), Anti-TRPC6 (1:100, Alomone,
916 ACC-017, RRID: AB_2040243, for Immunofluorescence), Anti-GAPDH (1:10000,
917 Santa Cruz, sc-137179,RRID: AB_2232048, for Western Blot), Anti-NALCN (1:100,
918 GeneTex, GTX54808, for Western Blot), Anti-TRPC6 (1:100, Cell Signaling
919 Technology, 16716, RRID:AB_2798768, for Western Blot).
920 Secondary antibodies: Donkey anti-Mouse IgG (H+L) Highly Cross-Adsorbed
921 Secondary Antibody (Alexa Fluor 488, Thermo Fisher Scientific, A-21202, 1:1000),
922 Donkey anti-Mouse IgG (H+L) Highly Cross-Adsorbed Secondary Antibody (Alexa
923 Fluor 546, Thermo Fisher Scientific, A10037, 1:1000), Donkey anti-Rabbit IgG (H+L)
924 Highly Cross-Adsorbed Secondary Antibody (Alexa Fluor 488, Thermo Fisher
925 Scientific, A21206, 1:1000), Donkey anti- Rabbit IgG (H+L) Highly Cross-Adsorbed
926 Secondary Antibody (Alexa Fluor 546, Thermo Fisher Scientific, A10040, 1:1000),

927 Donkey anti- Rabbit IgG (H+L) Highly Cross-Adsorbed Secondary Antibody (Alexa
928 Fluor 647, Thermo Fisher Scientific, A31573, 1:1000)
929
930 **Quantification and statistical analysis**
931 Software such as GraphPad Prism6, OriginPro 8.0 (Origin Lab) and Adobe Illustrator
932 CS6 were used for data analysis and image processing. All experimental data were
933 expressed as mean ± standard error (mean ± S.E.M.). When the data were normally
934 distributed, the difference between two groups was statistically analyzed by
935 two-sample T-test or paired-sample T-test; when the data were not normally
936 distributed, the difference between two groups was statistically analyzed by
937 Mann-Whitney U test or Wilcoxon matched-pairs signed rank test. $P < 0.05$ was
938 considered as a statistically significant difference between two groups. For the data
939 between multiple groups, when the data were normally distributed and there was no
940 significant variance in homogeneity, one-way ANOVA with Dunnett's multiple
941 comparisons test or two-way ANOVA with Sidak's multiple comparisons test was
942 used; when the data were not normally distributed, Kruslal-Wallis-H test with
943 Dunnett's multiple comparisons test and Student-Newman-Keuls test with Dunnett's
944 multiple comparisons test were used.
945
946 **Conflict of Interest**
947 The authors declare that the research was conducted in the absence of any commercial
948 or financial relationships that could be construed as a potential conflict of interest.
949 **Author Contributions**
950 Hailin Zhang conceived, designed and supervised the experiments; Jing Wang
951 performed the experiments, acquired and analyzed the data and prepared the figures;
952 Dongmei Zhang and Min Su performed immunofluorescence of the brain slices and
953 performed some preliminary electrophysiological experiments; Yuqi Sang and Chaoyi
954 Li performed part of single-cell PCR; Yongxue Zhang performed part of statistical
955 analysis; Ludi Zhang and Chenxu Niu took care of mice; Hailin Zhang and Jing Wang
956 wrote the manuscript; Hailin Zhang and Xiaona Du prepared the final version of the
957 manuscript.
958 **Funding**

This work was supported by the National Natural Science Foundation of China (81871075, 82071533) grants to HZ; National Natural Science Foundation of China (81870872) grants to XD; Science Fund for Creative Research Groups of Natural Science Foundation of Hebei Province (no. H2020206474);Basic Research Fund for Provincial Universities (JCYJ2021010), Natural Science Foundation of Hebei Province (H2023423065) and Scientific research project of Hebei administration of traditional Chinese Medicine (2024091) grants to WJ.

Acknowledgments

We would like to thank colleagues at the Core Facilities and Centers of Hebei Medical University for the technical assistance.

Data Availability Statement

The data that support the findings of this study are available from the corresponding author upon reasonable request.

References

1. Bromberg-Martin, E.S., M. Matsumoto, and O. Hikosaka, *Dopamine in motivational control: rewarding, aversive, and alerting.* Neuron, 2010. **68**(5): p. 815-34.
2. Lammel, S., B.K. Lim, and R.C. Malenka, *Reward and aversion in a heterogeneous midbrain dopamine system.* Neuropharmacology, 2014. **76 Pt B**(0 0): p. 351-9.
3. Van den Heuvel, D.M. and R.J. Pasterkamp, *Getting connected in the dopamine system.* Prog Neurobiol, 2008. **85**(1): p. 75-93.
4. Chaudhury, D., et al., *Rapid regulation of depression-related behaviours by control of midbrain dopamine neurons.* Nature, 2013. **493**(7433): p. 532-6.
5. Kabanova, A., et al., *Function and developmental origin of a mesocortical inhibitory circuit.* Nat Neurosci, 2015. **18**(6): p. 872-82.
6. Badrinarayan, A., et al., *Aversive stimuli differentially modulate real-time dopamine transmission dynamics within the nucleus accumbens core and shell.* J Neurosci, 2012. **32**(45): p. 15779-90.
7. Friedman, A.K., et al., *Enhancing depression mechanisms in midbrain dopamine neurons achieves homeostatic resilience.* Science, 2014. **344**(6181): p. 313-9.
8. Krishnan, V., et al., *Molecular adaptations underlying susceptibility and resistance to social defeat in brain reward regions.* Cell, 2007. **131**(2): p. 391-404.
9. Grace, A.A., et al., *Regulation of firing of dopaminergic neurons and control of goal-directed behaviors.* Trends Neurosci, 2007. **30**(5): p. 220-7.
10. Johnson, S.W. and R.A. North, *Two types of neurone in the rat ventral tegmental area and their synaptic inputs.* J Physiol, 1992. **450**: p. 455-68.
11. Zhong, P., et al., *HCN2 channels in the ventral tegmental area regulate behavioral responses to chronic stress.* Elife, 2018. **7**.

12. Bean, B.P., *The action potential in mammalian central neurons.* Nat Rev Neurosci, 2007. **8**(6): p. 451-65.
13. Guzman, J.N., et al., *Robust pacemaking in substantia nigra dopaminergic neurons.* J Neurosci, 2009. **29**(35): p. 11011-9.
14. Puopolo, M., E. Raviola, and B.P. Bean, *Roles of subthreshold calcium current and sodium current in spontaneous firing of mouse midbrain dopamine neurons.* J Neurosci, 2007. **27**(3): p. 645-56.
15. Khaliq, Z.M. and B.P. Bean, *Pacemaking in dopaminergic ventral tegmental area neurons: depolarizing drive from background and voltage-dependent sodium conductances.* J Neurosci, 2010. **30**(21): p. 7401-13.
16. Beckstead, M.J., et al., *Vesicular dopamine release elicits an inhibitory postsynaptic current in midbrain dopamine neurons.* Neuron, 2004. **42**(6): p. 939-46.
17. Ford, C.P., M.J. Beckstead, and J.T. Williams, *Kappa opioid inhibition of somatodendritic dopamine inhibitory postsynaptic currents.* J Neurophysiol, 2007. **97**(1): p. 883-91.
18. Philippart, F., et al., *Differential Somatic Ca2+ Channel Profile in Midbrain Dopaminergic Neurons.* J Neurosci, 2016. **36**(27): p. 7234-45.
19. Dufour, M.A., A. Woodhouse, and J.M. Goaillard, *Somatodendritic ion channel expression in substantia nigra pars compacta dopaminergic neurons across postnatal development.* J Neurosci Res, 2014. **92**(8): p. 981-99.
20. Kimm, T., Z.M. Khaliq, and B.P. Bean, *Differential Regulation of Action Potential Shape and Burst-Frequency Firing by BK and Kv2 Channels in Substantia Nigra Dopaminergic Neurons.* J Neurosci, 2015. **35**(50): p. 16404-17.
21. Li, L., et al., *Selective targeting of M-type potassium K(v) 7.4 channels demonstrates their key role in the regulation of dopaminergic neuronal excitability and depression-like behaviour.* Br J Pharmacol, 2017. **174**(23): p. 4277-4294.
22. Tarfa, R.A., R.C. Evans, and Z.M. Khaliq, *Enhanced Sensitivity to Hyperpolarizing Inhibition in Mesoaccumbal Relative to Nigrostriatal Dopamine Neuron Subpopulations.* J Neurosci, 2017. **37**(12): p. 3311-3330.
23. Seutin, V., et al., *Evidence for a modulatory role of Ih on the firing of a subgroup of midbrain dopamine neurons.* Neuroreport, 2001. **12**(2): p. 255-8.
24. Neuhoff, H., et al., *I(h) channels contribute to the different functional properties of identified dopaminergic subpopulations in the midbrain.* J Neurosci, 2002. **22**(4): p. 1290-302.
25. Krashia, P., et al., *On the properties of identified dopaminergic neurons in the mouse substantia nigra and ventral tegmental area.* Eur J Neurosci, 2017. **45**(1): p. 92-105.
26. Shi, Y., et al., *Nalcn Is a "Leak" Sodium Channel That Regulates Excitability of Brainstem Chemosensory Neurons and Breathing.* J Neurosci, 2016. **36**(31): p. 8174-87.
27. Lu, B., et al., *Peptide neurotransmitters activate a cation channel complex of NALCN and UNC-80.* Nature, 2009. **457**(7230): p. 741-4.
28. Philippart, F. and Z.M. Khaliq, *G(i/o) protein-coupled receptors in dopamine neurons inhibit the sodium leak channel NALCN.* Elife, 2018. **7**.
29. Lutas, A., et al., *The leak channel NALCN controls tonic firing and glycolytic sensitivity of substantia nigra pars reticulata neurons.* Elife, 2016. **5**.
30. Ford, N.C., D. Ren, and M.L. Baccei, *NALCN channels enhance the intrinsic excitability of spinal projection neurons.* Pain, 2018. **159**(9): p. 1719-1730.

1040 31. Um, K.B., et al., *TRPC3 and NALCN channels drive pacemaking in substantia nigra*
1041 *dopaminergic neurons.* Elife, 2021. **10**.
1042 32. Kim, S.H., et al., *Nonselective cation channels are essential for maintaining intracellular Ca2+*
1043 *levels and spontaneous firing activity in the midbrain dopamine neurons.* Pflugers Arch, 2007.
1044 **455**(2): p. 309-21.
1045 33. Zhou, F.W., S.G. Matta, and F.M. Zhou, *Constitutively active TRPC3 channels regulate basal*
1046 *ganglia output neurons.* J Neurosci, 2008. **28**(2): p. 473-82.
1047 34. Hof, T., et al., *Transient receptor potential channels in cardiac health and disease.* Nat Rev
1048 Cardiol, 2019. **16**(6): p. 344-360.
1049 35. Klipec, W.D., et al., *Loss of the trpc4 gene is associated with a reduction in cocaine*
1050 *self-administration and reduced spontaneous ventral tegmental area dopamine neuronal*
1051 *activity, without deficits in learning for natural rewards.* Behav Brain Res, 2016. **306**: p.
1052 117-27.
1053 36. German, D.C. and K.F. Manaye, *Midbrain dopaminergic neurons (nuclei A8, A9, and A10):*
1054 *three-dimensional reconstruction in the rat.* J Comp Neurol, 1993. **331**(3): p. 297-309.
1055 37. Nair-Roberts, R.G., et al., *Stereological estimates of dopaminergic, GABAergic and*
1056 *glutamatergic neurons in the ventral tegmental area, substantia nigra and retrorubral field in*
1057 *the rat.* Neuroscience, 2008. **152**(4): p. 1024-31.
1058 38. Cadwell, C.R., et al., *Electrophysiological, transcriptomic and morphologic profiling of single*
1059 *neurons using Patch-seq.* Nat Biotechnol, 2016. **34**(2): p. 199-203.
1060 39. Lammel, S., et al., *Unique properties of mesoprefrontal neurons within a dual*
1061 *mesocorticolimbic dopamine system.* Neuron, 2008. **57**(5): p. 760-73.
1062 40. Kawano, M., et al., *Particular subpopulations of midbrain and hypothalamic dopamine*
1063 *neurons express vesicular glutamate transporter 2 in the rat brain.* J Comp Neurol, 2006.
1064 **498**(5): p. 581-92.
1065 41. Stamatakis, A.M., et al., *A unique population of ventral tegmental area neurons inhibits the*
1066 *lateral habenula to promote reward.* Neuron, 2013. **80**(4): p. 1039-53.
1067 42. Lu, B., et al., *The neuronal channel NALCN contributes resting sodium permeability and is*
1068 *required for normal respiratory rhythm.* Cell, 2007. **129**(2): p. 371-83.
1069 43. Kusch, J., et al., *Interdependence of receptor activation and ligand binding in HCN2*
1070 *pacemaker channels.* Neuron, 2010. **67**(1): p. 75-85.
1071 44. Mistrík, P., et al., *The murine HCN3 gene encodes a hyperpolarization-activated cation*
1072 *channel with slow kinetics and unique response to cyclic nucleotides.* J Biol Chem, 2005.
1073 **280**(29): p. 27056-61.
1074 45. Clapham, D.E., L.W. Runnels, and C. Strübing, *The TRP ion channel family.* Nat Rev Neurosci,
1075 2001. **2**(6): p. 387-96.
1076 46. Urban, N., et al., *Identification and Validation of Larixyl Acetate as a Potent TRPC6 Inhibitor.*
1077 Mol Pharmacol, 2016. **89**(1): p. 197-213.
1078 47. Strübing, C., et al., *Formation of novel TRPC channels by complex subunit interactions in*
1079 *embryonic brain.* J Biol Chem, 2003. **278**(40): p. 39014-9.
1080 48. Goel, M., W.G. Sinkins, and W.P. Schilling, *Selective association of TRPC channel subunits in rat*
1081 *brain synaptosomes.* J Biol Chem, 2002. **277**(50): p. 48303-10.
1082 49. Tye, K.M., et al., *Dopamine neurons modulate neural encoding and expression of*
1083 *depression-related behaviour.* Nature, 2013. **493**(7433): p. 537-541.

1084 50. Chang, C.H. and A.A. Grace, *Amygdala-ventral pallidum pathway decreases dopamine activity*
1085 *after chronic mild stress in rats.* Biol Psychiatry, 2014. **76**(3): p. 223-30.
1086 51. Moreines, J.L., Z.L. Owrutsky, and A.A. Grace, *Involvement of Infralimbic Prefrontal Cortex but*
1087 *not Lateral Habenula in Dopamine Attenuation After Chronic Mild Stress.*
1088 Neuropsychopharmacology, 2017. **42**(4): p. 904-913.
1089 52. Willner, P., *The chronic mild stress (CMS) model of depression: History, evaluation and usage.*
1090 Neurobiol Stress, 2017. **6**: p. 78-93.
1091 53. Liu, D., et al., *Brain-derived neurotrophic factor-mediated projection-specific regulation of*
1092 *depressive-like and nociceptive behaviors in the mesolimbic reward circuitry.* Pain, 2018.
1093 **159**(1): p. 175.
1094 54. Kang, Y. and S.T. Kitai, *A whole cell patch-clamp study on the pacemaker potential in*
1095 *dopaminergic neurons of rat substantia nigra compacta.* Neurosci Res, 1993. **18**(3): p. 209-21.
1096 55. Lu, B., et al., *Extracellular calcium controls background current and neuronal excitability via*
1097 *an UNC79-UNC80-NALCN cation channel complex.* Neuron, 2010. **68**(3): p. 488-99.
1098 56. Benarroch, E.E., *HCN channels: function and clinical implications.* Neurology, 2013. **80**(3): p.
1099 304-10.
1100 57. Mercuri, N.B., et al., *Properties of the hyperpolarization-activated cation current Ih in rat*
1101 *midbrain dopaminergic neurons.* Eur J Neurosci, 1995. **7**(3): p. 462-9.
1102 58. Okamoto, T., M.T. Harnett, and H. Morikawa, *Hyperpolarization-activated cation current (Ih) is*
1103 *an ethanol target in midbrain dopamine neurons of mice.* J Neurophysiol, 2006. **95**(2): p.
1104 619-26.
1105 59. Chan, C.S., et al., *'Rejuvenation' protects neurons in mouse models of Parkinson's disease.*
1106 Nature, 2007. **447**(7148): p. 1081-6.
1107 60. Lee, J.H., L.L. Cribbs, and E. Perez-Reyes, *Cloning of a novel four repeat protein related to*
1108 *voltage-gated sodium and calcium channels.* FEBS Lett, 1999. **445**(2-3): p. 231-6.
1109 61. Lu, T.Z. and Z.P. Feng, *NALCN: a regulator of pacemaker activity.* Mol Neurobiol, 2012. **45**(3): p.
1110 415-23.
1111 62. Pochwat, B., et al., *Hyperforin Potentiates Antidepressant-Like Activity of Lanicemine in Mice.*
1112 Front Mol Neurosci, 2018. **11**: p. 456.
1113 63. Liu, Y., et al., *The change of spatial cognition ability in depression rat model and the possible*
1114 *association with down-regulated protein expression of TRPC6.* Behav Brain Res, 2015. **294**: p.
1115 186-93.
1116 64. Cao, J.L., et al., *Mesolimbic dopamine neurons in the brain reward circuit mediate*
1117 *susceptibility to social defeat and antidepressant action.* J Neurosci, 2010. **30**(49): p. 16453-8.
1118 65. Eder, P., et al., *Na(+) entry and modulation of Na(+)/Ca(2+) exchange as a key mechanism of*
1119 *TRPC signaling.* Pflugers Arch, 2005. **451**(1): p. 99-104.
1120 66. Hahn, S., et al., *Proximal dendritic localization of NALCN channels underlies tonic and burst*
1121 *firing in nigral dopaminergic neurons.* J Physiol, 2023. **601**(1): p. 171-193.
1122 67. Inoue, R. and Y. Mori, *Molecular candidates for capacitative and non-capacitative Ca2+ entry*
1123 *in smooth muscle.* Novartis Found Symp, 2002. **246**: p. 81-90; discussion 221-7.
1124 68. Nishida, M., et al., *Phosphorylation of TRPC6 channels at Thr69 is required for*
1125 *anti-hypertrophic effects of phosphodiesterase 5 inhibition.* J Biol Chem, 2010. **285**(17): p.
1126 13244-53.
1127 69. Nishioka, K., et al., *Cilostazol suppresses angiotensin II-induced vasoconstriction via protein*

kinase A-mediated phosphorylation of the transient receptor potential canonical 6 channel. Arterioscler Thromb Vasc Biol, 2011. **31**(10): p. 2278-86.

70. Su, M., et al., *Kv7.4 Channel Contribute to Projection-Specific Auto-Inhibition of Dopamine Neurons in the Ventral Tegmental Area.* Front Cell Neurosci, 2019. **13**: p. 557.

71. McCall, N.M., E. Marron Fernandez de Velasco, and K. Wickman, *GIRK Channel Activity in Dopamine Neurons of the Ventral Tegmental Area Bidirectionally Regulates Behavioral Sensitivity to Cocaine.* J Neurosci, 2019. **39**(19): p. 3600-3610.

72. Qu, N., et al., *A POMC-originated circuit regulates stress-induced hypophagia, depression, and anhedonia.* Mol Psychiatry, 2020. **25**(5): p. 1006-1021.

73. Butterweck, V., *Mechanism of action of St John's wort in depression : what is known?* CNS Drugs, 2003. **17**(8): p. 539-62.

74. Burlet, S., C.J. Tyler, and C.S. Leonard, *Direct and indirect excitation of laterodorsal tegmental neurons by Hypocretin/Orexin peptides: implications for wakefulness and narcolepsy.* J Neurosci, 2002. **22**(7): p. 2862-72.

75. Jan-Pieter and Konsman, *The mouse brain in stereotaxic coordinates: Second Edition (Deluxe) By Paxinos G. and Franklin, K.B.J., Academic Press, New York, 2001, ISBN 0-12-547637-X.* Psychoneuroendocrinology, 2003.

1147 **Figure legends**

1148 **Fig.1** The effects of extracellular Ca^{2+} and Na^{+} on firing activity of the male VTA DA
1149 neurons.

1150 **A**. Identification of the VTA DA neurons. i: confocal images showing the anatomical
1151 distribution of DA neurons in the VTA and SNc; the DA neurons were identified to be
1152 DAT-immunofluorescence positive (scale bar, 100 μm). ii: left panel: single-cell PCR
1153 results; four cells showed the presence of genes indicated. right panel: Percentage of
1154 neuronal markers (DA neuron: TH, DAT, D_2R, Girk2; Glu neuron: Vglut2 and GABA
1155 neuron: GAD1) positive neurons in the VTA neurons (GAPDH positive). n = 63 cells,
1156 N = 10. **B**. The effect of replacing extracellular Ca^{2+} with Mg^{2+} on firing frequency of
1157 the VTA DA neurons. Example time-course (i) and traces (ii) of the spontaneous
1158 firing before and after replacement of extracellular Ca^{2+} (2 mM) by an equimolar
1159 amount of Mg^{2+}.The inset on the top of ii shows a map of a coronal midbrain slice
1160 indicating the location of neurons that were recorded and subsequently identified as
1161 DA neurons which were DAT positive with single cell-PCR (red dots). iii:
1162 Summarized data for ii. Firing of the VTA DA neurons were recorded using loose
1163 cell-attached patch from a brain slice of the VTA (n = 16, N = 8). Paired-sample T test,
1164 t = 4.698, $P = 0.0003$. **C**. The effect of replacing extracellular Ca^{2+} with Mg^{2+} on the
1165 resting membrane potential (RMP) of the VTA DA neurons, in the presence of 1 μM
1166 TTX. Example time-course (i) and summarized data (ii) for the resting membrane
1167 potential before and after replacement of extracellular Ca^{2+} (2 mM) by an equimolar
1168 amount of Mg^{2+} (n = 14, N = 8). The inset on the top of ii shows a map of a coronal
1169 midbrain slice indicating the location of neurons that were recorded and subsequently
1170 identified as DA neurons which were DAT positive with single cell-PCR (red dots).
1171 Wilcoxon matched-pairs signed rank test, W = 66.00, $P = 0.037$. **D.** i: Replacement of
1172 external Na^{+} by equimolar NMDG resulted in hyperpolarization of the resting
1173 membrane potential of the VTA DA neurons, in the presence of 1 μM TTX. ii:
1174 Summarized data for i (n = 8, N = 5). The inset on the top of ii shows a map of a
1175 coronal midbrain slice indicating the location of neurons that were recorded and
1176 subsequently identified as DA neurons which were DAT positive with single cell-PCR
1177 (red dots). Paired-sample T test, t = 7.803, $P = 0.0001$. * $P < 0.05$, *** $P < 0.001$. n is
1178 number of neurons recorded and N is number of mice used.

1179

1180 **Fig. 2** Gene expression profile of non-selective cation channels (NSCCs) in the male
1181 VTA DA neurons.
1182 Single-cell RNA-Seq was performed on the VTA neurons projecting to five different
1183 brain regions of mice (NAc c, NAc ms, NAc ls, BLA, mPFC). **A**. Gene expression
1184 profile of markers for neuron subtypes from 45 VTA neurons; the neuron subtypes
1185 included: dopaminergic (Th, Ddc, DAT), GABAergic (Gad1, Gad2, VGAT) and
1186 glutamatergic (VGluT2, VGluT1, VGluT3), which was arranged in different rows
1187 indicated in the right labels and in the left-colored vertical lines; projection targets of
1188 these neurons were indicated at the top by the colored lines and labels. Relative
1189 expression levels of these genes were indicated by the dark-blue color intensity which
1190 was transformed from the log2 values of the number of transcripts per million (FPKM)
1191 plus 1. **B**. Relative gene expression levels of TRP channels (i) and other NSCCs (ii) in
1192 45 individual VTA DA neurons and the population average (mean, right columns).
1193 Each column of the individual neurons in (i) and (ii) corresponded to the columns in
1194 A. (iii) Bar graph of the mean log2 (FPKM +1) for the top 8 NSCCs in descending
1195 order. Error bars indicate SEM. **C.** Gene expression profile of aforementioned top 8
1196 NSCCs from 45 VTA neurons.
1197
1198 **Fig. 3** NALCN contributes to subthreshold depolarization and spontaneous firing of
1199 the male VTA DA neurons.
1200 **A**. Confocal images showing co-expression of NALCN (green) and DAT (red)
1201 representing DA neurons (scale bar, 10 μm). **B**. i: Single-cell PCR from the VTA DA
1202 neurons with the expression of NALCN. ii: Percentage of NALCN positive neurons
1203 from 15 DA neurons (with expression of DAT). **C**. Example time course (i) and
1204 summarized data (ii) showed that NALCN channel blockers ($GdCl_3$) significantly
1205 hyperpolarized the resting membrane potential (RMP) (n = 6, N = 6). The inset on the
1206 top of Cii shows a map of a coronal midbrain slice indicating the location of neurons
1207 that were recorded and subsequently identified as DA neurons which were DAT
1208 positive with single cell-PCR (red dots). Wilcoxon matched-pairs signed rank test, W
1209 = -21.00, P = 0.0313. **D**. Example time-course and traces (i) and summarized data (ii)
1210 of the effect of $GdCl_3$ on spontaneous firing frequency in DA neurons (n = 7, N = 3).
1211 The inset on the top of Dii shows a map of a coronal midbrain slice indicating the
1212 location of neurons that were recorded and subsequently identified as DA neurons

which were DAT positive with single cell-PCR (red dots). Paired-sample T test, t = 5.742, P = 0.0012. **E**. Example time course (i) and summarized data (ii) showed that NALCN channel blocker (L703,606) significantly hyperpolarized the resting membrane potential (RMP) (n = 6, N = 4). The inset on the top of Eii shows a map of a coronal midbrain slice indicating the location of neurons that were recorded and subsequently identified as DA neurons which were DAT positive with single cell-PCR (red dots). Paired-sample T test, t = 14.95, P = 0.0001. **F**. Example time-course and traces (i) and summarized data (ii) of the effect of L703,606 on spontaneous firing frequency in DA neurons (n = 8, N = 4). The inset on the top of Fii shows a map of a coronal midbrain slice indicating the location of neurons that were recorded and subsequently identified as DA neurons which were DAT positive with single cell-PCR (red dots). Paired-sample T test, t = 6.236, P = 0.0004. **G**. shRNA against NALCN carried by AAV virus (i) (NALCN-shRNA) was injected into the VTA of mice, the mRNA level in the shRNA-NALCN transfected VTA (NALCN-KD) and the scramble shRNA transfected VTA (Control) was analyzed using qPCR (ii) (N = 6). Two-sample T test, t = 3.742, P = 0.0038. **H**. Confocal images showing the expression of AAV9-NALCN-shRNA-GFP (green) in the VTA DA neurons (DAT, red) (scale bar, 10 μm). **I**. Loose cell-attached current clamp recordings of the spontaneous firing of the VTA DA neurons transfected with either NALCN-shRNA (ii, n = 12, N = 3) or scramble-shRNA (Con, i, n = 10, N = 3) (both GFP and DAT positive). Examples of firing traces in the middle of i and ii and summarized data in the bottom of i were shown. The inset on the top of i and ii shows a map of a coronal midbrain slice indicating the location of GFP^+ neurons that were recorded and subsequently identified as DA neurons which were DAT positive with single cell-PCR (i: Con, grey dots; ii: NALCN-KD, red dots). Mann-Whitney U test, U = 0, P = 0.0001. **J**. Whole-cell current clamp recordings of the resting membrane potential (RMP) of the VTA DA neurons transfected with either NALCN-shRNA (NALCN-KD, ii, n = 18, N = 5) or scramble-shRNA (Con, i, n = 15, N = 5) (both GFP and DAT positive). Examples of RMP in the middle of i and ii and summarized data in the bottom of i were shown. The inset on the top of i and ii shows a map of a coronal midbrain slice indicating the location of GFP^+ neurons that were recorded and subsequently identified as DA neurons which were DAT positive with single cell-PCR (i: Con, grey dots; ii: NALCN-KD, red dots). Mann-Whitney U test, U = 0, P = 0.0001. * $P < 0.05$,

1246 ** P <0.01, *** P < 0.001. n is number of neurons recorded and N is number of mice
1247 used.
1248
1249 **Fig. 4** TRP channels contribute to subthreshold depolarization and spontaneous firing
1250 of the male VTA DA neurons.
1251 **A**. The expression of TRP channels in VTA DA neurons. i: Single-cell PCR from 5
1252 VTA cells (C1-C5). ii: Percentage of TRP channels (C3, C6 and V2) positive neurons
1253 in the VTA DA neurons (DAT positive). **B** and **C**. Example time-course (i), traces (ii)
1254 and the summarized data (iii) for the effect of a nonselective cation channel blocker
1255 2-APB (100 μM, n = 12, N = 5) (B) and a potent TRPC6 inhibitor LA (10 μM, n = 7,
1256 N = 5) (C) on the spontaneous firing frequency in the VTA DA neurons. The inset on
1257 the top of Bii and Cii shows a map of a coronal midbrain slice indicating the location
1258 of neurons that were recorded and subsequently identified as DA neurons which were
1259 DAT positive with single cell-PCR (red dots). B: Wilcoxon matched-pairs signed rank
1260 test, W = -78.00, P = 0.0005. C: Paired-sample T test, t = 4.089, P = 0.0064. **D** and **E.**
1261 Example time-course (i) and the summarized data (ii) for the effect of a nonselective
1262 cation channel blocker 2-APB (n = 6, N = 6) (D) and a potent TRPC6 inhibitor LA (n
1263 = 5, N = 4) (E) on the resting membrane potential (RMP) of the VTA DA neurons.
1264 Paired-sample T test, D: t = 7.976, P = 0.0005, E: t = 5.610, P = 0.005. ** P < 0.01,
1265 *** P < 0.001. n is number of neurons recorded and N is number of mice used.
1266
1267 **Fig. 5** TRPC6 contributes to subthreshold depolarization and spontaneous firing of the
1268 male VTA DA neurons.
1269 **A**. The normalized expression profile of TRPC6 in NAc c- and mPFC-projecting VTA
1270 DA neurons was verified using single cell-qPCR (NAc c: n = 28, N = 7; mPFC: n =
1271 25, N = 8, both TH positive), Mann-Whitney U test, U = 174, P = 0.0014. **B**.
1272 Confocal images showing co-expression of TRPC6 (green) and TH (red) representing
1273 DA neurons (scale bar, 10 μm). **C**. The efficiency of shRNA knockdown of TRPC6 in
1274 the VTA verified by qPCR. shRNA against TRPC6 carried by AAV virus (i)
1275 (TRPC6-shRNA) was injected into the VTA of mice, the mRNA level in the
1276 shRNA-TRPC6 transfected VTA (TRPC6-KD, N = 5) and the scramble shRNA
1277 transfected VTA (Con, N = 5) was analyzed using qPCR (ii). Two-sample T test,
1278 t=4.184, P=0.0031. **D**. Immunofluorescence labelling showing the expression of

AAV9-shRNA (TRPC6)-GFP (green) and DAT (red) in the VTA (scale bar, 10 μm). **E**. Loose cell-attached current clamp recordings of the spontaneous firing of the VTA DA neurons from the mice transfected with either TRPC6-shRNA (TRPC6-KD, ii, n = 9, N = 3) or scramble-shRNA (Con, i, n = 9, N = 3) (both GFP and DAT positive). Examples of firing traces in the middle of i and ii and summarized data in the bottom of ii were shown. The inset on the top of i and ii shows a map of a coronal midbrain slice indicating the location of GFP^+ neurons that were recorded and subsequently identified as DA neurons which were DAT positive with single cell-PCR (i: Con, grey dots; ii: TRPC6-KD, red dots). Two-sample T test, t = 3.005, P = 0.0084. **F**. Example time-course (i) and summarized data (ii) showed that shRNA knockdown of TRPC6 in the VTA decreased the 2-APB-inhibited firing responses of the VTA DA neurons. The inset on the top of ii shows a map of a coronal midbrain slice indicating the location of GFP^+ neurons that were recorded and subsequently identified as DA neurons which were DAT positive with single cell-PCR (TRPC6-KD, red dots). (n = 7, N = 5, both GFP and DAT positive), Wilcoxon matched-pairs signed rank test, W = -18.00, P = 0.1563. **G**. Whole-cell current clamp recordings of the resting membrane potential (RMP) of the VTA DA neurons transfected with either TRPC6-shRNA (TRPC6-KD, ii, n = 10, N = 6) or scramble-shRNA (Con, i, n = 10, N = 6) (both GFP and DAT positive). Examples of RMP in the middle of i and ii and summarized data in the bottom of i were shown. The inset on the top of i and ii shows a map of a coronal midbrain slice indicating the location of GFP+ neurons that were recorded and subsequently identified as DA neurons which were DAT positive with single cell-PCR (i: Con, grey dots; ii: TRPC6-KD, red dots). Mann-Whitney U test, U = 8, P = 0.0007. **H**. Example time-course (i) and summarized data (ii) showed that shRNA knockdown of TRPC6 in the VTA decreased the LA-inhibited firing responses of the VTA DA neurons. The inset on the top of ii shows a map of a coronal midbrain slice indicating the location of GFP^+ neurons that were recorded and subsequently identified as DA neurons which were DAT positive with single cell-PCR (TRPC6-KD, red dots). (n = 8, N = 5, both GFP and DAT positive), Paired-sample T test, t = 0.000, P = 0.9999. n.s. $P > 0.05$, ** $P < 0.01$, *** $P < 0.001$. n is number of neurons recorded and N is number of mice used.

Fig. 6 CMUS depression male mice have a decreased firing activity and

down-regulated TRPC6 expression in the VTA DA neurons.

A. Experimental procedure timeline. **B**. i: Sucrose preference test for CMUS mice. Two-sample T test, t = 5.810, P = 0.0001, compared with control mice. ii: Tail suspension test for CMUS mice, Two-sample T test, t = 4.689, P = 0.0005, compared with control mice. **C**. Loose cell-attached current clamp recordings of the spontaneous firing of the VTA DA neurons from the CMUS (n = 28, N = 5, DAT positive) and the control (n = 18, N = 5, DAT positive) mice. The inset on the top of i and ii shows a map of a coronal midbrain slice indicating the location of neurons that were recorded and subsequently identified as DA neurons which were DAT positive with single cell-PCR (i: Con, grey dots; ii: CMUS, red dots). Examples of firing traces in the bottom of i as well as in the bottom left of ii and summarized data in the bottom right of ii were shown. Mann-Whitney U test, U = 118, P = 0.0020. **D**. Representative Western blot assay (i) and summarized data (ii) showing the expression of TRPC6 and GAPDH in the VTA of the control (Con, N = 6) and the CMUS (N = 6) mice. Two-sample T test, t = 4.848, P = 0.0007. **E**. i and ii: Example traces (up) and time-course (bottom) of firing frequency of mPFC-projecting VTA DA neurons, effect of 2-APB. (i) Con, (ii) CMUS. iii. Summarized effect of 2-APB in the control (n = 12 cells, N = 5, DAT positive) and CMUS (n = 15 cells, N=5, DAT positive) mice. Two-way ANOVA with Sidak's multiple comparisons test, Con *vs*. CMUS: $F_{(1, 25)}$ = 3.411, Con-ACSF *vs*. CMUS-ACSF, P = 0.0001; Con-2-APB *vs*. CMUS-2-APB, P = 0.0164. ACSF *vs*. 2-APB: $F_{(1, 25)}$ = 92.43, Con-ACSF *vs*. Con-2-APB, P = 0.0001; CMUS-ACSF *vs*. CMUS-2-APB, P = 0.2259. iv. The inhibition rate (%) on firing rate by 2-APB in the control group (n = 12, N=5) and the CMUS group (n = 15, N = 5). Mann-Whitney U test, U = 1, P = 0.0001. The inset on the top of iii and iv shows a map of a coronal midbrain slice indicating the location of mPFC-projecting neurons that were recorded and subsequently identified as DA neurons which were DAT positive with single cell-PCR (iii: Con, grey dots; iv: CMUS, red dots). **F**. i and ii: Example traces (up) and time-course (bottom) of firing frequency of mPFC-projecting VTA DA neurons, effects of LA.(i) Con, (ii) CMUS. iii. Summarized effect of LA on the control (n = 17 cells, N = 8, DAT positive) and CMUS (n = 19 cells, N = 8, DAT positive) mice. Kruslal-Wallis-H test with Dunnett's multiple comparisons test, H = 53.08, Con-ACSF *vs*. Con-LA: P = 0.0001, Con-ACSF *vs*. CMUS-ACSF: P = 0.0023, CON-LA *vs.* CMUS-LA: P = 0.0187, CMUS-ACSF *vs*. CMUS-LA: P > 0.9999. iv.

The inhibition rate (%) on firing rate by LA in the control group (n = 17, N = 8) and the CMUS group (n = 19, N = 8). Mann-Whitney U test, U = 0, $P = 0.0001$. The inset on the top of iii and iv shows a map of a coronal midbrain slice indicating the location of mPFC-projecting neurons that were recorded and subsequently identified as DA neurons which were DAT positive with single cell-PCR (iii: Con, grey dots; iv: CMUS, red dots). n.s. $P > 0.05$, * $P < 0.05$, ** $P < 0.01$, *** $P < 0.001$. n is number of neurons recorded and N is the number of mice used.

Fig. 7 Selective knockdown of TRPC6 in the VTA DA neurons confers the male mice with depression-like and anxiety-like behaviors which are reversed by overexpression of TRPC6.

A. shRNA against TRPC6 carried by AAV-loxp virus (TRPC6-shRNA) was injected into the VTA of the DAT-Cre mice. **B**. The mRNA level in the shRNA-TRPC6 transfected VTA (TRPC6-cKD) and the scramble shRNA transfected VTA (Con) was analyzed using qPCR (Con: N = 4; TRPC6-cKD: N = 6). Mann-Whitney U test, U = 0, $P = 0.0159$. **C**. Immunofluorescence labelling showing the expression of AAV9-hSyn-DIO-shRNA (TRPC6)-RFP (red) and DAT (green) in the VTA of the DAT-Cre mice (scale bar, 10 μm). **D**. The effects of Cre-induced conditional knockdown of TRPC6 in the VTA DA neurons on the behaviors of mice in the sucrose preference test (i), the tail suspension test (ii), and the elevated plus-maze test (iii, iv) (Con: N = 9; TRPC6-cKD: N = 13). Two-sample T test, Sucrose preference test: t = 4.663, $P = 0.0001$; Tail suspension test: t = 7.143, $P = 0.0001$; Elevated plus-maze test: open arm t = 10.36, $P = 0.0001$, closed arm t = 11.18, $P = 0.0001$.**E**. The effects of TRPC6 over-expression. AAV9-DIO-TRPC6-GFP (TRPC6-cOE) was injected into the VTA of the DAT-Cre mice, 7 days after TRPC6 knocking down (AAV9-hSyn-DIO-shRNA (TRPC6)-RFP injection). **F**. The protein level TRPC6 of VTA (Con: the scramble shRNA for TRPC6, N = 7; C6-cKO: TRPC6-cKD, N = 8; c6-cKO+cOE: TRPC6-cKD+ TRPC6-cOE, N = 7). Kruskal-Wallis H test with Dunnett's multiple comparisons test, H = 14.75, Con *vs.* C6-cKO: $P = 0.0016$, C6-cKO *vs.* C6-cKO+cOE: $P = 0.0062$. **G**. Immunofluorescence labelling showing the expression of AAV9-hSyn-DIO-shRNA (TRPC6)-RFP (red), AAV9-DIO-TRPC6-GFP (green) and DAT (blue) in the VTA of the DAT-Cre mice (scale bar, 10 μm). **H**. The effects of TRPC6 over-expression on depression-like

behaviors of TRPC6-cKD mice: the sucrose preference test (i), the tail suspension test (ii), and the elevated plus-maze test (iii) (Con: N = 11; TRPC6-cKD: N = 11; TRPC6-cKD+TRPC6-cOE: N = 11). One-way ANOVA with Dunnett's multiple comparisons test, sucrose preference test: $F_{(2, 30)} = 37.22$, Con *vs.* C6-cKO: $P = 0.0001$, C6-cKO *vs.* C6-cKO+cOE: $P = 0.0001$; tail suspension test: $F_{(2, 30)} = 20.10$, Con *vs.* C6-cKO: $P = 0.0146$, C6-cKO *vs.* C6-cKO+cOE: $P = 0.0001$; elevated plus-maze test: $F_{(2, 30)} = 17.10$, Con *vs.* C6-cKO: $P = 0.0001$, C6-cKO *vs.* C6-cKO+cOE: $P = 0.0095$. * $P < 0.05$, ** $P < 0.01$, *** $P < 0.001$.n is number of neurons recorded and N is the number of mice used.

Fig. 8 Selective knockdown of TRPC6 in the mPFC-projecting VTA DA neurons produces depression-like and anxiety-like behaviors.

A. shRNA against TRPC6 carried by retro-AAV-loxp virus (TRPC6-shRNA) was injected into the mPFC of the DAT-Cre male mice. **B**. The mRNA level in the shRNA-TRPC6 transfected VTA (TRPC6-rcKD) DA neurons and the scramble shRNA transfected VTA DA neurons (Con) was analyzed using single-cell quantitative PCR (scqPCR) (Con: n = 8, N = 4; TRPC6-rcKD: n = 10, N = 4). Two-sample T test, t = 4.506, $P = 0.0004$. **C**. Immunofluorescence labelling showing the expression of AAV-retro-hSyn-DIO-mCherry-shRNA (TRPC6) (red) and DAT (green) in the VTA of the DAT-Cre mice (scale bar, 10 μm). **D**. The effects of Cre-induced conditional knockdown of TRPC6 in mPFC-projecting VTA DA neurons on the behaviors of mice: (i) the sucrose preference test, (ii) the tail suspension test, and (iii) the elevated plus-maze test (Con: N = 8; TRPC6-rcKD: N = 10). Two-sample T test, sucrose preference test: t = 5.215, $P = 0.0001$; tail suspension test: t = 2.993, $P = 0.0097$; elevated plus-maze test: open arm t = 5.802, $P = 0.0001$. ** $P < 0.01$, *** $P < 0.001$. n is number of neurons recorded and N is the number of mice used.

Fig. 1

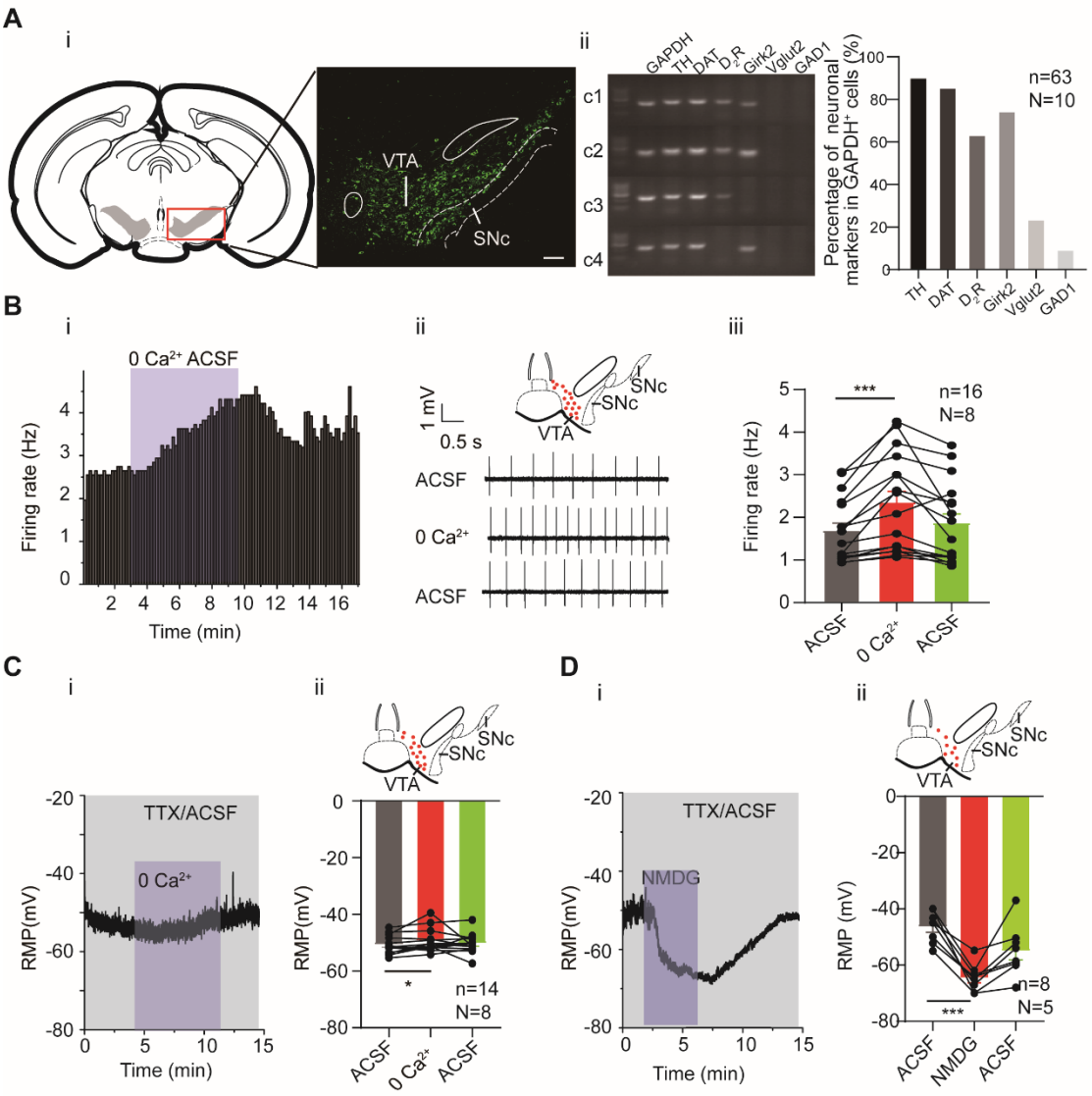
A
i
VTA
SNc
ii
GAPDH
TH
DAT
D2R
Girk2
Vglut2
GAD1
c1
c2
c3
c4
Percentage of neuronal markers in GAPDH+ cells (%)
n=63
N=10
TH
DAT
D2R
Girk2
Vglut2
GAD1
B
i
0 Ca2+ ACSF
Firing rate (Hz)
Time (min)
ii
1 mV
0.5 s
SNc
VTA
ACSF
0 Ca2+
ACSF
iii
***
n=16
N=8
Firing rate (Hz)
ACSF
0 Ca2+
ACSF
C
i
TTX/ACSF
0 Ca2+
RMP(mV)
Time (min)
ii
SNc
VTA
RMP(mV)
*
n=14
N=8
ACSF
0 Ca2+
ACSF
D
i
TTX/ACSF
NMDG
RMP(mV)
Time (min)
ii
SNc
VTA
RMP (mV)
***
n=8
N=5
ACSF
NMDG
ACSF

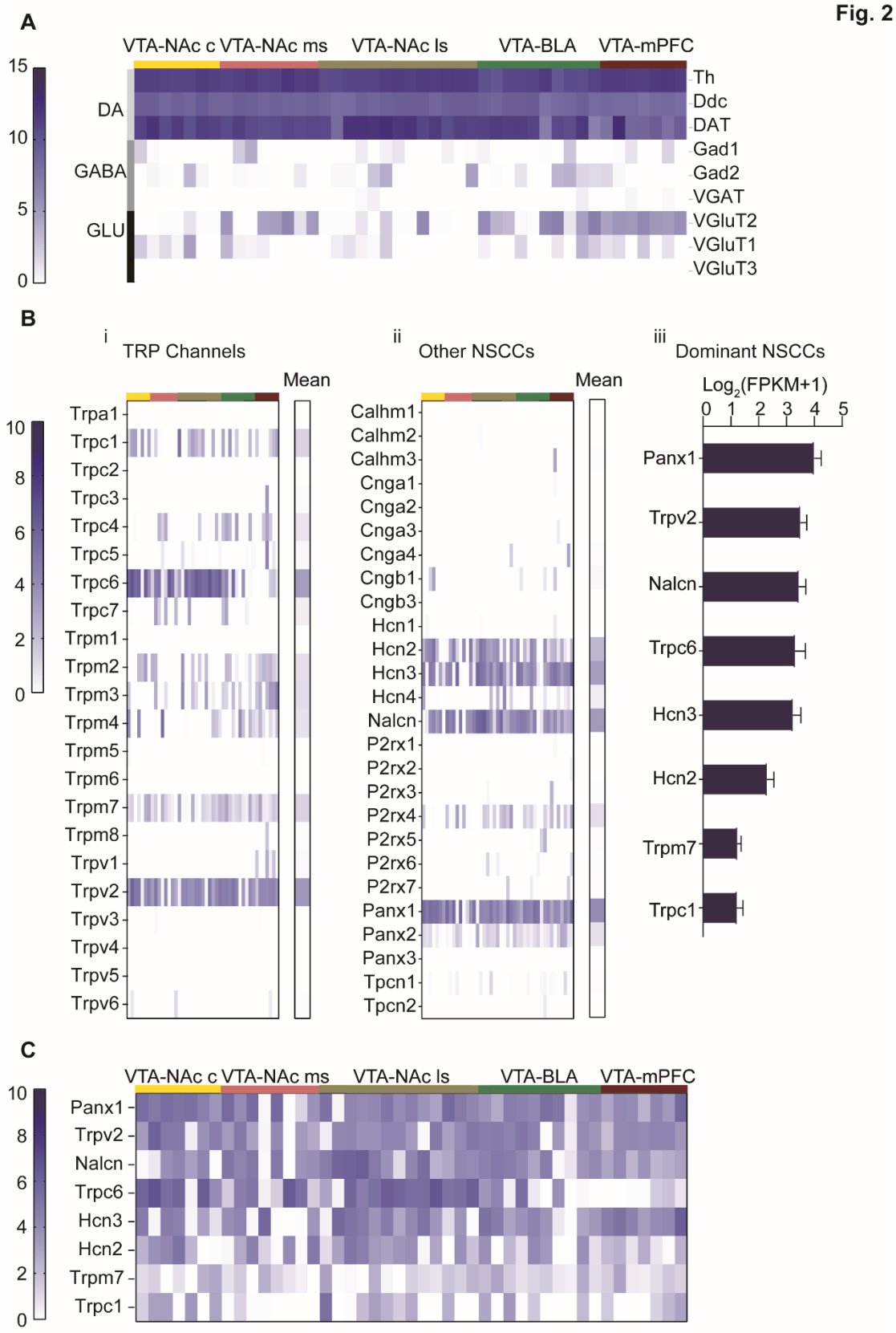
Fig. 2
A
VTA-NAc c
VTA-NAc ms
VTA-NAc ls
VTA-BLA
VTA-mPFC
DA
GABA
GLU
Th
Ddc
DAT
Gad1
Gad2
VGAT
VGluT2
VGluT1
VGluT3
B
i
TRP Channels
ii
Other NSCCs
iii
Dominant NSCCs
Mean
Log2(FPKM+1)
Trpa1
Trpc1
Trpc2
Trpc3
Trpc4
Trpc5
Trpc6
Trpc7
Trpm1
Trpm2
Trpm3
Trpm4
Trpm5
Trpm6
Trpm7
Trpm8
Trpv1
Trpv2
Trpv3
Trpv4
Trpv5
Trpv6
Calhm1
Calhm2
Calhm3
Cnga1
Cnga2
Cnga3
Cnga4
Cngb1
Cngb3
Hcn1
Hcn2
Hcn3
Hcn4
Nalcn
P2rx1
P2rx2
P2rx3
P2rx4
P2rx5
P2rx6
P2rx7
Panx1
Panx2
Panx3
Tpcn1
Tpcn2
C

Fig. 3

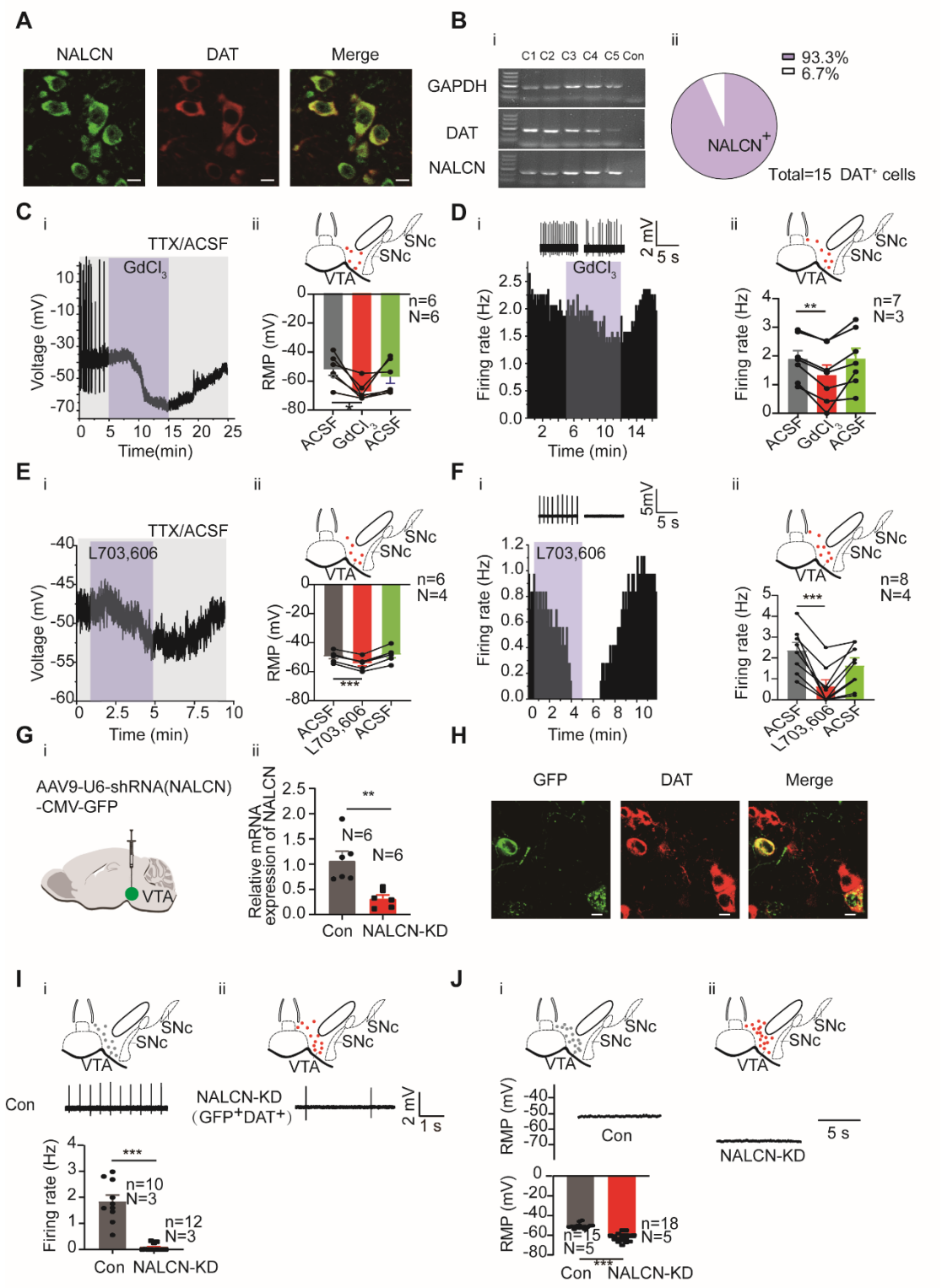
A
NALCN
DAT
Merge
B
i
C1 C2 C3 C4 C5 Con
GAPDH
DAT
NALCN
ii
93.3%
6.7%
NALCN+
Total=15 DAT+ cells
C
i
TTX/ACSF
GdCl3
Voltage (mV)
Time(min)
ii
SNc
VTA
RMP (mV)
n=6
N=6
ACSF
GdCl3
ACSF
D
i
2 mV
5 s
GdCl3
Firing rate (Hz)
Time (min)
ii
n=7
N=3
E
i
TTX/ACSF
L703,606
Voltage (mV)
Time (min)
ii
n=6
N=4
L703,606
F
i
5mV
5 s
L703,606
Firing rate (Hz)
Time (min)
ii
n=8
N=4
G
i
AAV9-U6-shRNA(NALCN)
-CMV-GFP
VTA
ii
Relative mRNA expression of NALCN
N=6
N=6
Con
NALCN-KD
H
GFP
DAT
Merge
I
i
SNc
VTA
Con
ii
NALCN-KD
(GFP+DAT+)
2 mV
1 s
Firing rate (Hz)
n=10
N=3
n=12
N=3
Con
NALCN-KD
J
i
ii
RMP (mV)
Con
NALCN-KD
5 s
n=15
N=5
n=18
N=5
Con
NALCN-KD

1419

1420

Fig. 4

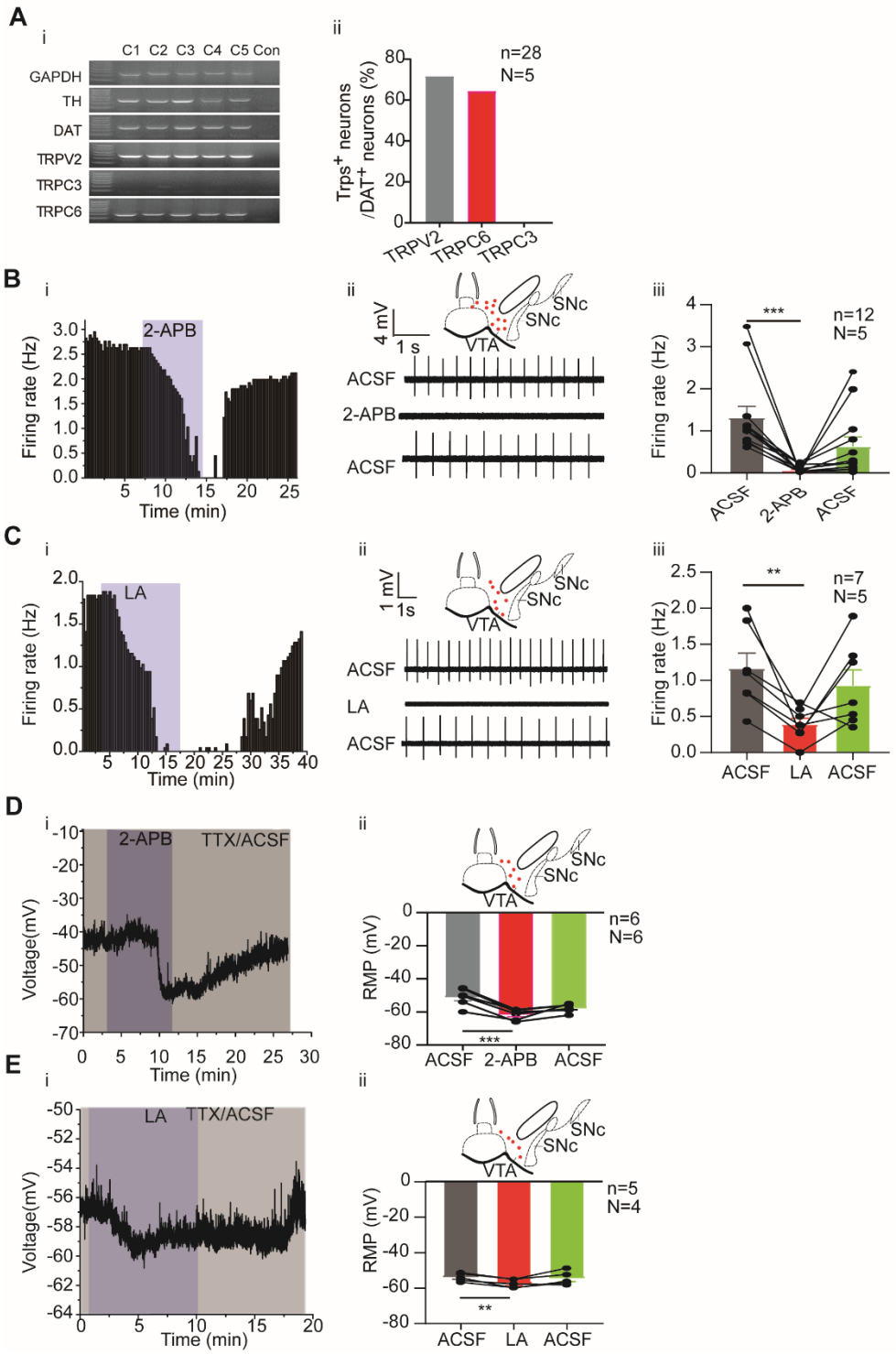

1421

1422

1423

1424

1425

Fig. 5

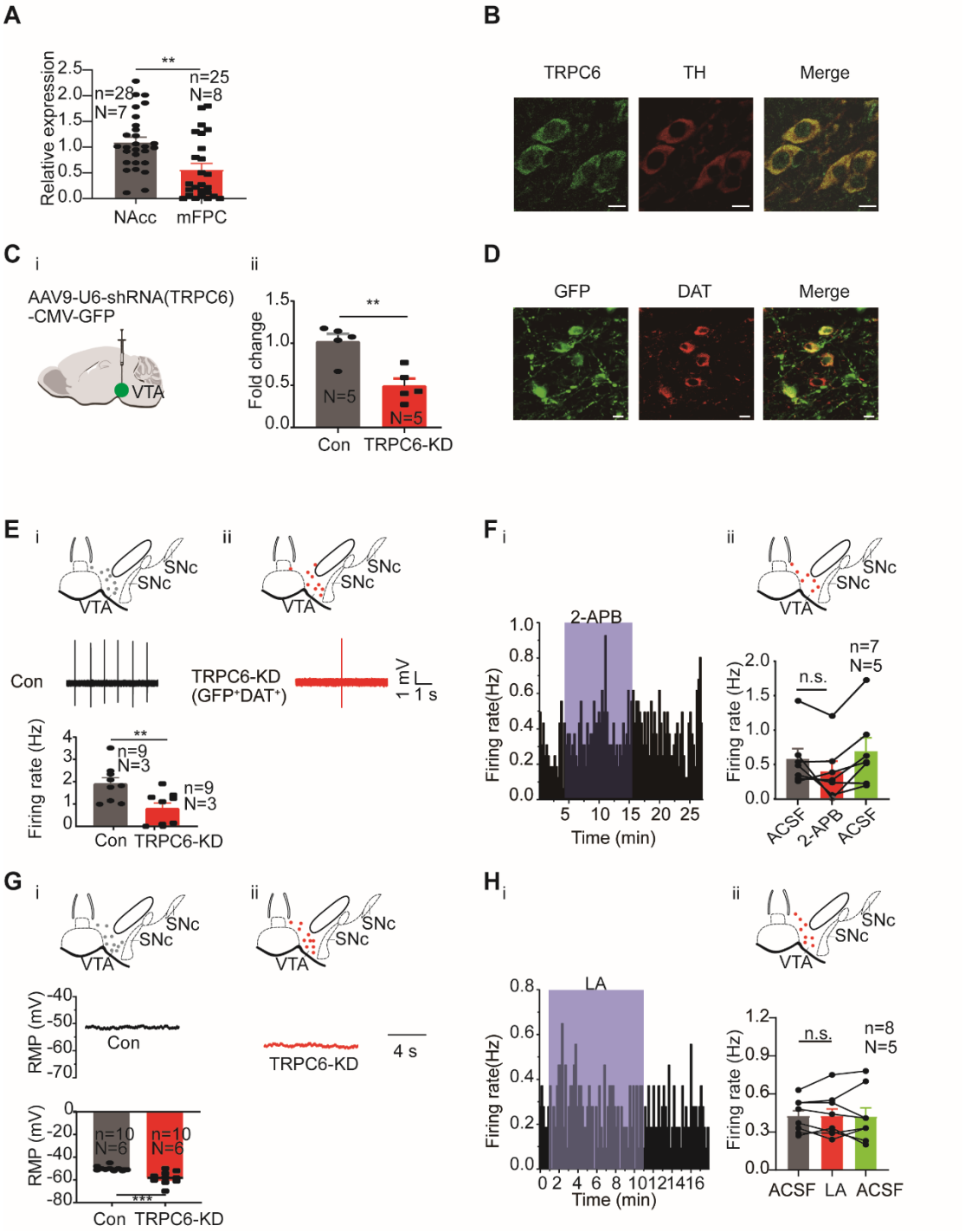

1426

1427

1428

1429

1430

1431

Fig. 6

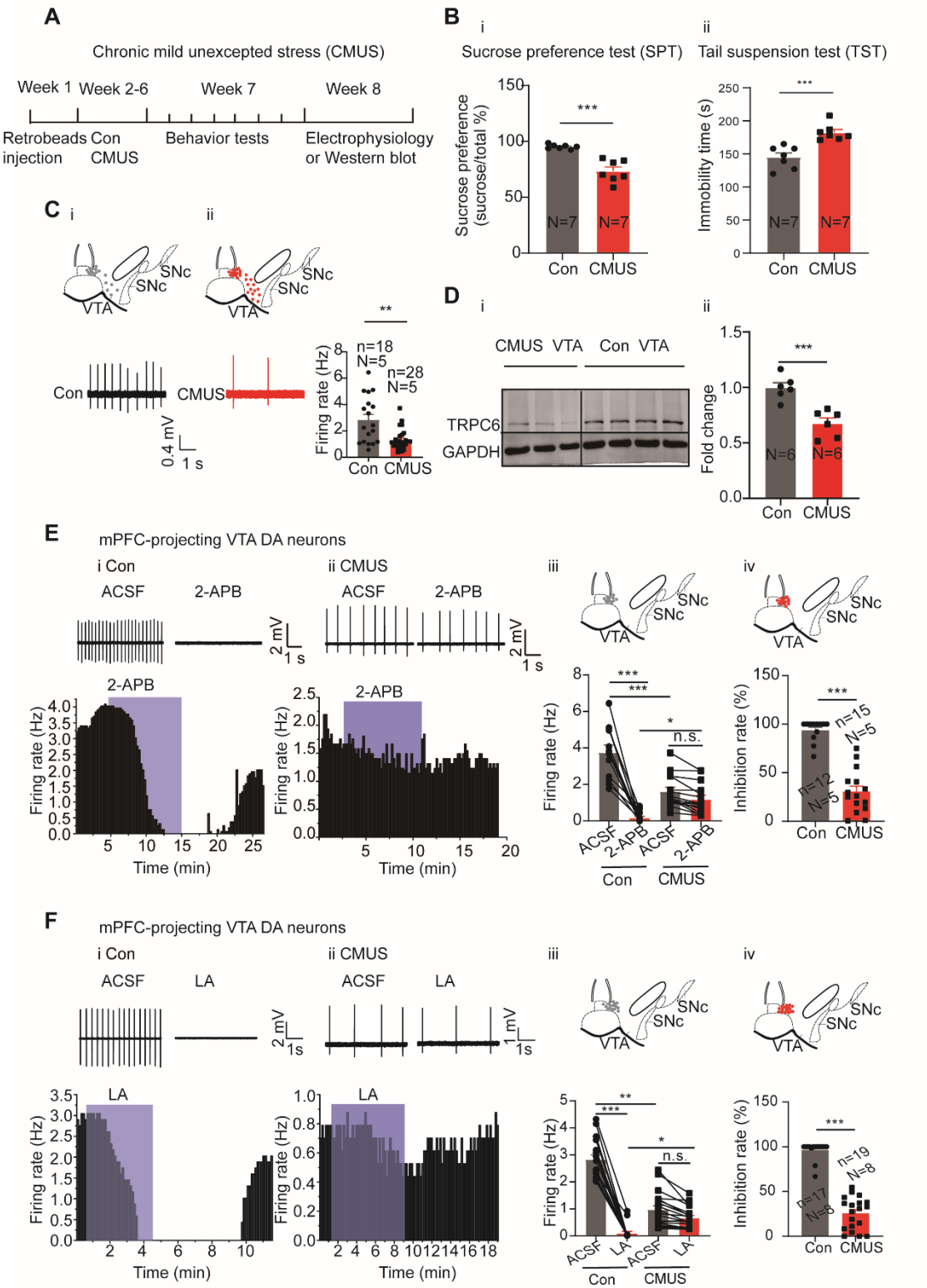

1432

1433

1434

1435

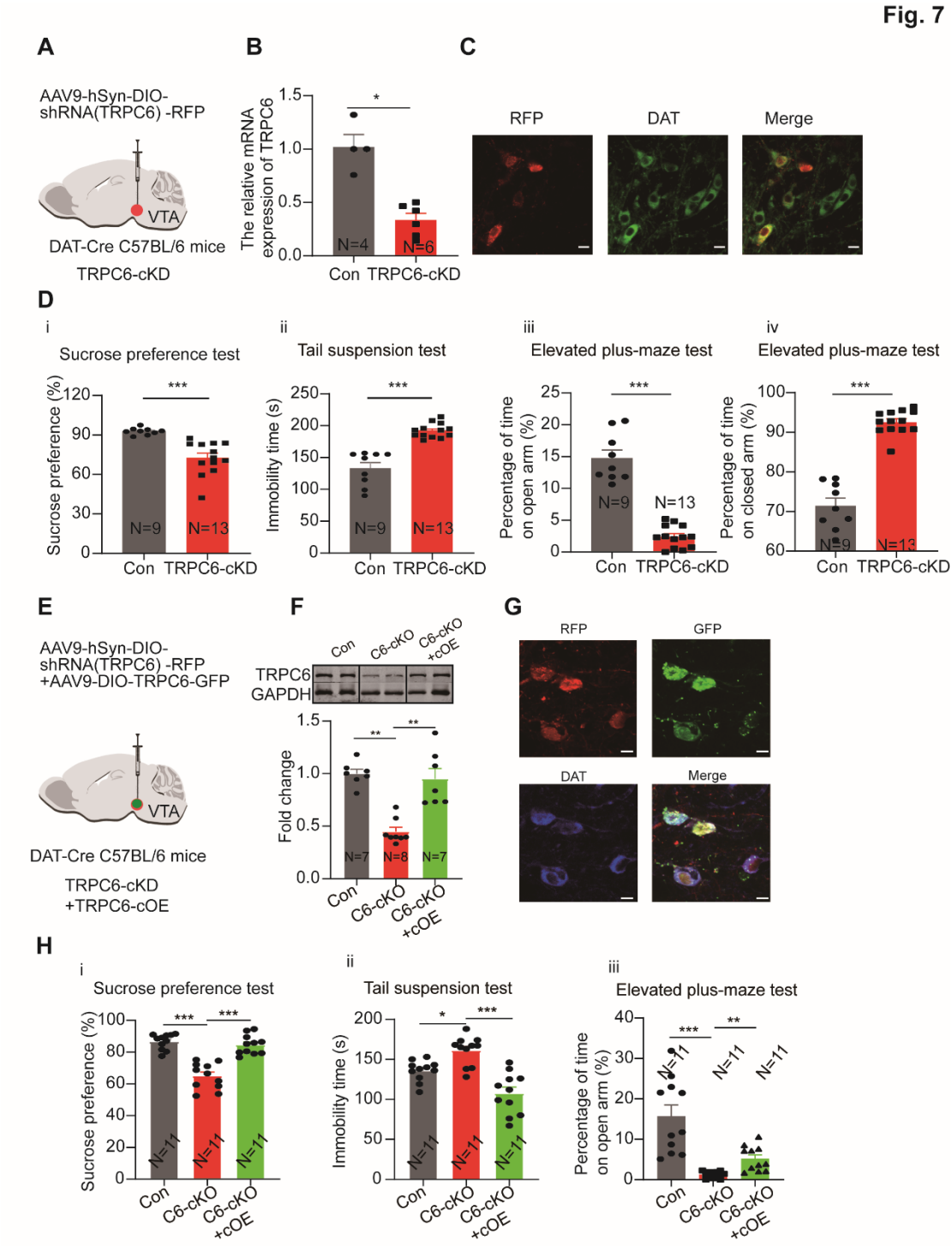

1436

1437

1438

1439

1440

1441

1442

Fig. 8

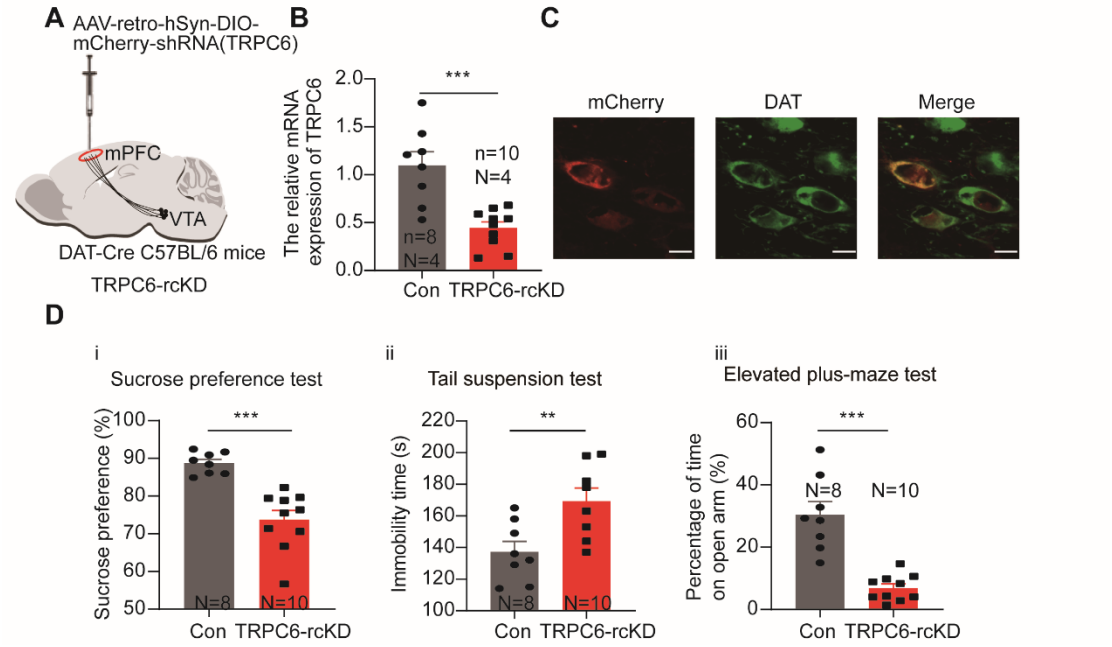

1443